1 Adaptive Depth and Pitch Control of an Underwater Vehicle with Real-Time Experiments

Divine Maalouf, Ahmed Chemori, Vincent Creuze

$\mathcal{L}_1$ Adaptive Depth and Pitch Control of an Underwater Vehicle with Real-Time Experiments

Divine Maalouf, Ahmed Chemori, Vincent Creuze

LIRMM,Univ.Montpellier2-CNRS, 161 rue Ada, 34392 Montpellier, France

Abstract

This paper proposes a new control scheme for underwater vehicles. These systems are highly nonlinear and they often operate in a varying environment. A robust controller is therefore needed to deal with these challenges. The recently developped $\mathcal{L}_1$ adaptive controller is proposed to be designed and implemented in real time for the first time on an underwater vehicle. Different experimental scenarios are then conducted to test the performance of the closed-loop system in two degrees of freedom. An interesting particularity of this controller lies in its architecture where robustness and adaptation are decoupled enabling thus high adaptation gains. This would result in a fast adaptation with a guaranteed smooth transient response without any persistency of excitation. In order to validate the choice of this controller, a comparative study is proposed to be conducted with the well proven adaptive nonlinear state feedback controller (ANSF). Real-time experimental results are proposed for different scenarios including nominal case, external disturbances rejection and robustness towards parameters uncertainties.

URL: ahmed.chemori@lirmm.fr (Vincent Creuze), phone number: 0033647094162 (Vincent Creuze)

This comparative study highlights clearly the superiority of the $\mathcal{L}_1$ adaptive controller.
Keywords: Adaptive Control, Autonomous Systems, Underwater vehicles, Robustness, Experimentations.

---

1. Introduction

Underwater vehicles have gained an increased interest in the last decades given the multiple tasks they can accomplish in various fields ranging from scientific to industrial and military applications. For this reason, it is less risky and more advantageous to send robots in hazardous environments such as deep seas and oceans. In our study, we are particularly interested in the category of tethered underwater vehicles also called Remotely Operated Vehicles (ROV). Different challenges in autonomous control of such systems arise from the inherent high nonlinearities and time varying behavior of the vehicle's dynamics subject to hydrodynamic effects and external disturbances. To deal with these problems, various advanced control techniques have been proposed in litterature such as robust $\mathcal{H}_\infty$ approaches (Roche et al., 2011), backstepping control (Lapierre & Soetanto, 2007), predictive control (Steenson et al., 2012) and sliding mode control (Pisano & Usai, 2004). Intelligent control methods using reinforcement learning or artifical intelligence have also been proposed (Kim & Yuh, 2001)(Chang et al., 2003)(Carreras et al., 2002). A more detailed overview of the proposed controllers for underwater vehicles can be found in (Yuh, 2000) and (Yildiz et al., 2009). In all of these cited articles, the need for robustness and adaptation is

highlighted since the robot's parameters are hard to identify and the environment where it operates is likely to change. For example, the addition of sensors or payloads modifies the weight and the position of the center of mass of the vehicle, furthermore the experimental conditions vary whether the vehicle operates in a sea or in a river resulting in a different buoyancy for each case. In order to avoid a degradation in the performance of the controlled system during a specific mission, the vehicle is expected to possess a self tuning ability and compensate for different kind of disturbances. That is why adaptive controllers are very popular for such systems (Fjellstad & Fossen, 1994a)(Antonelli et al., 1999)(Antonelli, 2003)(Antonelli, 2006). Since adaptation was found to be a necessity, it was combined with other techniques such as sliding mode control (Fossen & Sagatun, 1991), fuzzy logic control (Marzbanrad et al., 2011) or backstepping control (Lapierre, 2009). However, various problems are related to the implementation of an adaptive controller on an underwater vehicle. For instance, we notice that most of these adaptive schemes require regressor matrices based on a knowledge of the dynamic model and a large set of parameters to be estimated. In order to remediate to this problem, some non-regressor based controllers emerged such as the one proposed in (Yuh et al., 1999) also detailed in (Yuh & Nie, 2000) where a combination of unknown bounded constants are estimated. In (Zhao & Yuh, 2000), a disturbance observer has been added to the initial controller of (Yuh & Nie, 2000) and interesting experimental results have been obtained in nominal conditions as well as in case of external disturbances rejection and robustness towards parameters' uncertainties. The advantage of this method is that it does not require any *a priori*

knowledge about the system; furthermore the update of the parameters is based on the performances of the closed-loop system. However, the drawbacks of such a method lies in the neglect of the coupling effects between the degrees of freedom due to the spherical shape of the used robot. The model parameters of the dynamic model can be initialized randomly, but the control parameters governing this method are very critical to be tuned and highly dependent on the initial configuration of the robot. In (Sun & Chea, 2003), an adaptive control scheme based on a saturated proportional derivative feedback law was proposed for a setpoint control case. The contribution of this last paper lies in the use of only one regressor being for gravity instead of a full regressor for the whole dynamic model. In addition to that, an approximation was made when the transpose of the transformation matrix between the body frame and the earth frame was used instead of its inverse. Six adaptive controllers, including the three previously cited (Fjellstad & Fossen, 1994a)(Yuh & Nie, 2000)(Sun & Chea, 2003), were compared in (Antonelli, 2007) in simulation within a study that focuses on the ability of the controllers to compensate for the persistent effects (restoring forces and ocean currents). The non-regressor-based methods (Yuh & Nie, 2000)(Sun & Chea, 2003) were unable to compensate for the restoring forces and the model-based methods (Fjellstad & Fossen, 1994a)(Fossen & Balchen, 1991)(Fjellstad & Fossen, 1994b) needed adequate persistent excitation. This will generate a problem at steady state when a static error occurs in presence of waves or current. Indeed, in this scenario, the parameter excitation will be reduced since the error on the velocity is zero while the position error is not, and therefore a corrective adaptive con-

trol action cannot be triggered. The adaptive control law introduced in (Antonelli et al., 2001) was the one defended in the comparative study of (Antonelli, 2007) because it accomplishes the desired full compensation, however it still requires the adaptation of nine parameters with a suitable initialization of the restoring parameter vector and a reasonable choice for the adaptation gain. The simulations were performed on an ellipsoidal autonomous vehicle weighing 225kg. Another comparative study between adaptive controllers was made in (Fossen & Fjellstad, 1996) where the two adaptive controllers previously presented in (Slotine & Benedetto, 1990) and (Sadegh & Horowitz, 1990) were compared in simulations in presence of unknown model parameters and noisy measurements. The conclusion was that by replacing the regressor with the desired state trajectories in (Sadegh & Horowitz, 1990) a better robustness towards measurement noise was noticed. All of the previously cited papers on adaptive schemes reveal that despite their numerous advantages, these controllers hold some drawbacks that have been highlighted above for our specific application. Without a loss of generality, we notice that the same problems are present in other applications and therefore based on the above discussion we can list some of the main commun drawbacks of adaptive control:

i) A wide range of such controllers exhibit undesirable frequency characteristics and are often used with restrictive assumptions (Rohrs et al., 1982). The authors showed that sinusoidal reference inputs at certain frequencies and/or sinusoidal output disturbances at any frequency will cause the adaptation gain to significantly increase which will destabilize the control system.

ii) The need for the persistency in excitation can lead to a bad transient behavior (Zang & Bitmead, 1990).

iii) An increase in the adaptation gain drives the closed-loop system closer to instability while a small gain would slow down the convergence rate (Narendra & Annaswamy, 1987).

iv) Any parameter vector to be adapted must be adequately initialized and this choice would depend on the specific configuration of the system. This would be even more critical for the non-model-based controllers (Antonelli, 2007).

That is why a control approach that can ensure a robustness decoupled from adaptation would be highly desirable. Such a scheme would drive the closed-loop system to its desired trajectory while overcoming the drawbacks listed above. This decoupling has recently been proven to be achievable by the $\mathcal{L}_1$ adaptive control scheme presented in (Hovakimyan & Cao, 2010). It can be compared to a Model Reference Adaptive Controller (MRAC) modified in two ways: a state predictor is used instead of a reference model and a low-pass filter is inserted in the feedback loop to cancel out undesirable high frequencies in the control input. This controller can ensure a good performance with zero parameter initialization and without any necessity for a specific excitation. It is worth to note that, to the best knowledge of the authors, this control scheme was mainly applied to aerial vehicles (Dobrokhodov et al., 2010)(Kaminer et al., 2010) and mechatronic systems (Techy et al., 2007)(Fan & Smith, 2008) and has never been applied yet to underwater vehicles. We propose in this paper the theoretical aspects of the de-

sign of an $\mathcal{L}_1$ adaptive controller to be applied for the first time on an underwater vehicle. Moreover, we experimentally compare this new controller, in underwater robotics, with the well proven nonlinear state feedback controller proposed in (Fossen, 2002). Various scenarios allow us to compare each controller's performances in nominal conditions and in presence of external disturbances, as well as their robustness towards parameter uncertainties. Furthermore, the vehicles used in the previously cited papers are significantly bigger and heavier than the one used for our study (it weighs only 3kg). Indeed, a small vehicle is more sensitive to any kind of disturbance compared to a larger one thus placing us in difficult experimental conditions. The tether alone, given its weight and diameter relative to the dimensions of the robot, constitutes in itself a persistant disturbance to be compensated. This paper is an extension of the work presented in (Maalouf et al., 2012) where only depth and pitch were controlled with an $\mathcal{L}_1$ adaptive controller. In the actual work, not only new experimental results are introduced to highlight the capacity of the $\mathcal{L}_1$ adaptive controller to reject external disturbances, but a thorough quantitative comparative study with the nonlinear adaptive state feedback controller is also provided for different experimental scenarios. This study emphasizes the superiority of the $\mathcal{L}_1$ adaptive controller in terms of fast adaptation and robustness. This paper is organized as follows: in the second section we present the dynamic modeling of the system, the third section describes the two proposed control schemes, the forth section presents the prototype and its experimental setup, in the fifth section the obtained experimental results will be presented and discussed, and in the sixth section the performance of the two

controllers will be analyzed and compared. Finally the paper ends with some concluding remarks.

2. Dynamic modeling of the underwater vehicle

2.1. Modeling Background

The dynamics of an underwater vehicle involves two frames of reference: the body-fixed frame and the earth-fixed frame (cf. Figure 1). The vectors with the variables put at stake are $\nu = [u, v, w, p, q, r]^T$ and $\eta = [x, y, z, \phi, \vartheta, \psi]^T$ being the vectors of velocities (in the body-fixed frame) and position/Euler angles (in the earth-fixed frame) respectively. By considering the inertial generalized forces, the hydrodynamic effects, the gravity, and buoyancy contributions as well as the effects of the actuators (i.e thrusters), the dynamic model of an underwater vehicle in matrix form, using the SNAME notation and the representation described in (Fossen, 2002), can be written as follows:

$$\dot{\eta} = J(\eta)\nu \tag{1}$$

$$M\dot{\nu} + C(\nu)\nu + D(\nu)\nu + g(\eta) = \tau + w_d \tag{2}$$

$J(\eta) \in \mathbb{R}^{6\times6}$ is the transformation matrix mapping the body-fixed frame to the earth-fixed one. The model matrices M, C, and D denote inertia (including added mass), Coriolis-centripetal (including added mass), and damping respectively, while g is a vector of gravitational/buoyancy forces. τ is the vector of control

inputs and w_d the vector of external disturbances. In the case of our study, the vehicle used has a slow dynamics, and hence it will be moving at velocities low enough to make the Coriolis terms negligible ($C(\nu) \approx 0$). Considering this assumption, the dynamics (2) can be rewritten as:

$$M\dot{\nu} + n(\nu, \eta) = \tau + w_d \tag{3}$$

with $n(\nu, \eta) = D(\nu)\nu + g(\eta)$.

Equation (2) describes the dynamics of the system in 6 degrees of freedom taking into account the 3 translations and 3 rotations. The input vector $\tau \in \mathbb{R}^6$ considers 6 actions on the system to fully control it. The presented formulation of the robot's dynamics is expressed in the body-fixed frame and can be transformed to the earth-fixed frame by using the kinematic transformations of the state variables and the model parameters as follows:

$$\begin{aligned}
\dot{\eta} &= J(\eta)\nu \\
\ddot{\eta} &= J(\eta)\dot{\nu} + \dot{J}(\eta)\nu \\
M^*(\eta) &= J^{-T}(\eta)\, M\, J^{-1}(\eta) \\
D^*(\nu, \eta) &= J^{-T}(\eta)\, D(\nu)\, J^{-1}(\eta) \\
g^*(\eta) &= J^{-T}(\eta)\, g(\eta) \\
\tau^* &= J^{-T}(\eta)\, \tau \\
w_d^* &= J^{-T}(\eta)\, w_d
\end{aligned} \tag{4}$$

Equation (2) can therefore be expressed in the earth fixed frame as:

$$M^*(\eta)\ddot{\eta} + D^*(\nu,\eta)\dot{\eta} + g^*(\eta) = \tau^* + w_d^* \tag{5}$$

2.2. Modeling of the Studied Dynamics

The previous section describes the dynamics of an underwater vehicle in its full six degrees of freedom. In this paper, the proposed controllers will target two degrees of freedom due to the limitations we have in terms of sensors and actuators. Therefore, we have chosen to study a trajectory of motion in depth which is the vertical translational motion (along the z axis) and in pitch ϑ which is the rotation around the y axis. In fact, the inertial measurement unit (IMU) is the only sensor giving information concerning surge and sway (translational motion along x and y respectively). This information is the acceleration which is not enough to give an adequate estimate of the needed position values: integrations need to be done leading to a drift that cannot be corrected since no other sensor is available on board for this purpose. On the other hand, yaw measurement cannot be used due to the very short distance between the magnetic sensor and motors inducing strong magnetic disturbances. Due to the small size of the vehicle, this distance cannot be increased. The roll is not actuated in this robot and therefore we were left with the depth and pitch to control. These two degrees of freedom are coupled and hold high nonlinearities. For this reason, in the case where the adequate instrumentation would be available (i.e. x, y, and yaw measurements), the controller could easily be extended to other degrees of freedom. We can easily extract our

studied dynamics from (2) to get the reduced model of interest in the body-fixed frame as:

$$\begin{bmatrix} M_z & 0 \\ 0 & M_\vartheta \end{bmatrix}\begin{bmatrix} \dot{w} \\ \dot{q} \end{bmatrix}+\begin{bmatrix} D_z & 0 \\ 0 & D_\vartheta \end{bmatrix}\begin{bmatrix} w \\ q \end{bmatrix}+\begin{bmatrix} -cos(\varphi)cos(\vartheta)(W-B) \\ Wr_{g_z}sin(\vartheta) \end{bmatrix}=\begin{bmatrix} \tau_z + w_{d_z} \\ \tau_\vartheta + w_{d_\vartheta} \end{bmatrix} \quad (6)$$

The matrices of mass and damping constituted of the terms M_z, M_ϑ and D_z, D_ϑ respectively are considered as diagonal given the symmetrical cubic shape of our robot. W is the weight of the robot, B its buoyancy and r_{g_z} is the z coordinate of the robot's center of mass. $\tau_r = \begin{bmatrix} \tau_z \\ \tau_\vartheta \end{bmatrix}$ is expressed in Newton and is given by:

$$\tau_r = TKu \quad (7)$$

where $u \in \mathbb{R}^2$ is the vector of control inputs in volts generated by the two vertical thrusters acting simultaneously on the depth and pitch, K is the force coefficient in Newton/Volt that has been identified after several tests performed on the motors. $T \in \mathbb{R}^{2\times2}$ is the actuators configuration matrix taking into account the position and orientation of the motors, thus allowing to determine the associated forces in the body frame.

Similarly, we extract from (5) the studied dynamics in the earth frame to be:

$$\begin{bmatrix} M_z^* & 0 \\ 0 & M_\vartheta^* \end{bmatrix}\begin{bmatrix} \ddot{z} \\ \ddot{\vartheta} \end{bmatrix}+\begin{bmatrix} D_z^* & 0 \\ 0 & D_\vartheta^* \end{bmatrix}\begin{bmatrix} \dot{z} \\ \dot{\vartheta} \end{bmatrix}+\begin{bmatrix} -(W-B) \\ Wr_{g_z}cos(\varphi)sin(\vartheta) \end{bmatrix}=\begin{bmatrix} \tau_z^* + w_{d_z}^* \\ \tau_\vartheta^* + w_{d_\vartheta}^* \end{bmatrix} \quad (8)$$

All the starred terms can be computed in a straightforward manner using transformations in (4).

3. Proposed adaptive control schemes

Before introducing the design of the proposed $\mathcal{L}_1$ adaptive controller, we briefly remind the design of the well-known Adaptive Nonlinear State Feedback Controller (ANSF) and its formulation to our application. In fact, this well proven controller will be used in our experiments as a basis of comparison in order to highlight the performances of the $\mathcal{L}_1$ adaptive controller. In the rest of the paper, the subscript r in the model matrices refers to the reduced model (8) pertaining to the studied dynamics.

3.1. Adaptive Nonlinear State Feedback Controller

3.1.1. Background

The adaptive state feedback controller provides an online estimation of the unknown model parameters in order to ensure a good trajectory following by the closed-loop system (Fossen, 2002). The control law obtained based on the dynamics of the robot presented in equation (3) and given by:

$$\tau = \hat{M}a^b + \hat{n}(\nu, \eta) \tag{9}$$

where the hat symbol denotes the parameters' estimates, a^b the commanded acceleration described in the body-fixed frame, and $\hat{n}(\nu, \eta)$ the estimate of $n(\nu, \eta)$ in

(3). Given that the dynamic model is linear in its parameters, the adaptive control law (9) can then be rewritten as:

$$\tau = \Phi(a^b, \nu, \eta)\,\hat{\theta} \tag{10}$$

where Φ is the regressor matrix and $\hat{\theta}$ is the vector of the estimated parameters. The computed input is calculated in the body-fixed frame but the trajectory following is performed in the earth-fixed frame and therefore a^b is calculated from a simple transformation between the body and the earth fixed frames and is given by:

$$a^b = J^{-1}(a^n - \dot{J}\nu) \tag{11}$$

where a^n is the commanded acceleration in the earth-fixed frame and J the transformation matrix from the body-fixed frame to the earth-fixed frame with $\dot{J}$ its first derivative. To guarantee that the error converges to zero, a^n is chosen as follows:

$$a^n = \ddot{\eta}_{des} - K_P\tilde{\eta} - K_I\int_0^t \tilde{\eta}\,dt - K_D\dot{\tilde{\eta}} \tag{12}$$

with $\tilde{\eta} = \eta - \eta_{des}$ and $\dot{\tilde{\eta}}$ is its first derivative, η_{des} is the desired trajectory and $\ddot{\eta}_{des}$ is its corresponding acceleration.

The vector of the estimated parameters is updated according to the following update law:

$$\dot{\hat{\theta}} = -\Gamma\Phi^T(a^b, \nu, \eta)J^{-1}y_A \tag{13}$$

where Γ is a diagonal positive definite matrix representing the adaptation gain, and y_A the combined error defined as follows:

$$y_A = c_0\tilde{\eta} + c_1\dot{\tilde{\eta}} \tag{14}$$

c_0 and c_1 are constant positive gains. The choice of their values is governed by the algorithm presented in (Fossen, 2002) guaranteeing the convergence of the error to zero. The proof of stability is made by applying Barbalat's lemma.

3.1.2. Application to the studied dynamics

The vector of parameters to be estimated includes the elements of the matrices M_r^* and D_r^* and the parameters in the vector g_r^*. From equations (9) to (14), we extract the explicit formulation of our controller as:

$$\tau_r = \Phi_r\hat{\theta}_r \tag{15}$$

with the vector of the estimated parameters being:

$$\hat{\theta}_r = \begin{bmatrix} \hat{M}_z & \hat{D}_z & \widehat{W-B} & \hat{M}_\vartheta & \hat{D}_\vartheta & x_G\widehat{W-x_BB} & z_G\widehat{W-z_BB} \end{bmatrix}^T \tag{16}$$

$(W - B)$ is the parameter representing the difference between the weight and the buoyancy. x_G and z_G are the coordinates of the center of gravity in the body-fixed frame and x_B and z_B are the ones of the center of buoyancy. Given that the origin

of our body-fixed frame is in fact the center of buoyancy and that we consider both centers of gravity and buoyancy aligned due to the symmetry of the robot, we have $x_G = x_B = z_B = 0$ and we can therefore simplify our parameters' vector to the following:

$$\hat{\theta}_r = \begin{bmatrix} \hat{M}_z & \hat{D}_z & \widehat{W-B} & \hat{M}_\vartheta & \hat{D}_\vartheta & \widehat{z_G W} \end{bmatrix}^T \tag{17}$$

with this simplification taken into account, the regressor matrix takes the form:

$$\Phi_r = \begin{bmatrix} a_z^b & w & -cos(\vartheta)cos(\varphi) & 0 & 0 & 0 \\ 0 & 0 & 0 & a_\vartheta^b & q & sin(\vartheta) \end{bmatrix} \tag{18}$$

the commanded acceleration in the earth frame is given by:

$$a_r^n = \begin{bmatrix} \ddot{z}_{des} \\ \ddot{\vartheta}_{des} \end{bmatrix} - K_P \begin{bmatrix} z - z_{des} \\ \vartheta - \vartheta_{des} \end{bmatrix} - K_I \int_0^t \begin{bmatrix} z - z_{des} \\ \vartheta - \vartheta_{des} \end{bmatrix} dt - K_D \begin{bmatrix} \dot{z} - \dot{z}_{des} \\ \dot{\vartheta} - \dot{\vartheta}_{des} \end{bmatrix} \tag{19}$$

K_P, K_I and $K_D \in \mathbb{R}^{2\times 2}$ are diagonal positive constant matrices representing respectively the proportional, the integral and the derivative gains. The commanded acceleration in the body-fixed frame is:

$$a_r^b = \begin{bmatrix} cos(\varphi)cos(\vartheta) & 0 \\ 0 & cos(\varphi) \end{bmatrix}.$$

$$\left(a_r^n - \begin{bmatrix} -qsin(\vartheta) - pcos(\vartheta)sin(\varphi) & 0 \\ 0 & -\dot{\varphi}sin(\varphi) \end{bmatrix} \begin{bmatrix} w \\ q \end{bmatrix} \right) \tag{20}$$

the parameters adaptation law writes:

$$\dot{\hat{\theta}}_r = -\Gamma_r \Phi_r^T \begin{bmatrix} cos(\varphi)cos(\vartheta) & 0 \\ 0 & cos(\varphi) \end{bmatrix} y_{A_r} \tag{21}$$

the combined error is expressed by:

$$y_{A_r} = c_0 \begin{bmatrix} z - z_{des} \\ \vartheta - \vartheta_{des} \end{bmatrix} + c_1 \begin{bmatrix} \dot{z} - \dot{z}_{des} \\ \dot{\vartheta} - \dot{\vartheta}_{des} \end{bmatrix} \tag{22}$$

Finally, given the configuration matrix T and the force coefficient K explained in equation (7) the control input will take the form:

$$u = \frac{T^{-1}\tau_r}{K} \tag{23}$$

It is important to emphasize that a good parameter convergence is more guaranteed to occur when the reference trajectory is rich enough to excite the parameters to be estimated (Slotine & Weiping, 1991). These parameters will converge to a set of values that allows trajectory following. Moreover, the vector of parameters is seen to be bounded according to Barbalat's lemma as shown in the proof of stability given by (Fossen, 2002).

3.2. $\mathcal{L}_1$ adaptive controller

3.2.1. Background

To control the system described in (5), an $\mathcal{L}_1$ adaptive controller is proposed. The choice of this controller is motivated by its architecture characterized by the decoupling between adaptation and robustness. High adaptation gains can then be chosen securing a fast convergence with a smooth transient response. This architecture described in (Hovakimyan & Cao, 2010) is shown in the following block-diagram (cf. Figure 2). The closed-loop system holds a prediction phase and an adaptation phase. In the feebdack, a low pass filter is added to cancel out the high frequencies that might occur in the control input. This last component ensures fast adaptation without harming the robustness. The details of the different blocks of Figure 2 are the following:

- Controlled System: We will start by considering the following class of nonlinear systems which including our underwater vehicle:

$$\begin{aligned} \dot{x}_1(t) &= x_2(t) & x_1(0) &= x_{1_0} \\ \dot{x}_2(t) &= f(t, x(t)) + B_2\omega u & x_2(0) &= x_{2_0} \\ y(t) &= Cx(t) \end{aligned} \tag{24}$$

  where $x_1 \in \mathbb{R}^n$ and $x_2 \in \mathbb{R}^n$ are the states of the system forming the complete state vector: $x(t) = [x_1^T(t),\ x_2^T(t)]^T$. $u(t) \in \mathbb{R}^m$ is the control input vector ($m \leq n$) and $\omega \in \mathbb{R}^{m\times m}$ is the uncertainty on the input gain. $B_2 \in \mathbb{R}^{n\times m}$ is a constant full rank matrix. $C \in \mathbb{R}^{m\times n}$ is a known full rank constant ma-

trix, $y \in \mathbb{R}^m$ is the vector of measured outputs and $f(t, x(t))$ is an unknown nonlinear function representing the nonlinear dynamics. The partial derivatives of this function are assumed to be semiglobaly uniformly bounded and $f(t, 0)$ is assumed to be bounded. The previous system of equations can be transformed into a semi linear one with some assumptions on the boundedness of the parameters and function $f(t, x(t))$ as described in (Cao & Hovakimyan, 2008). It is concluded that this function can be rewritten as $f(t, x(t) = A_2 x_2 + \theta(t)||x(t)||_{\mathcal{L}_\infty} + \sigma(t)$ with $\theta(t)$ and $\sigma(t)$ unknown varying parameters. Therefore the system can be rewritten as follows:

$$\dot{x}(t) = \begin{bmatrix} 0_{n\times n} & \mathbb{I}_n \\ 0_{n\times n} & A_2 \end{bmatrix} \begin{bmatrix} x_1 \\ x_2 \end{bmatrix} + \begin{bmatrix} 0_{n\times 1} \\ \theta \end{bmatrix} ||x||_{\mathcal{L}_\infty} + \begin{bmatrix} 0_{n\times 1} \\ \sigma \end{bmatrix} + \begin{bmatrix} 0_{n\times m} \\ B_2 \end{bmatrix} \omega u \tag{25}$$

$$y(t) = Cx(t) \tag{26}$$

Let $A = \begin{bmatrix} 0_{n\times n} & \mathbb{I}_n \\ 0_{n\times n} & A_2 \end{bmatrix}$ be the state matrix describing the actual open-loop system dynamics. It should be modified into a Hurwitz matrix describing the desired closed-loop dynamics using a static feedback gain k_m. We would therefore get $A_m = A - B_m k_m$ with $B_m = \begin{bmatrix} 0_{n\times m} \\ B_2 \end{bmatrix}$. The system can then be

finally rewritten in compact form as:

$$\begin{aligned} \dot{x}(t) &= A_m x(t) + B_m\Big(\omega u_a + \theta(t)\|x(t)\|_{\mathcal{L}_\infty} + \sigma(t)\Big); \quad x(0) = x_0 \\ y(t) &= Cx(t) \end{aligned} \tag{27}$$

Given their structure, the vectors θ and σ can be summed to the control input as shown above. In case the vector B_2 is not an identity matrix, these two uncertain varying parameters would be scaled by the constants contained in B_2. Since they are unknown, the notation for these two variables will not be changed. u_a is the control input used for adaptation after the transformation of the matrix A into A_m. The final control input to be applied to the system is $u = u_m + u_a$ with $u_m = -k_m\, x$.

- State Predictor: The states of the system are calculated at each iteration using the estimated parameters obtained from the adaptation phase along with the control input. The prediction equation is then written as:

$$\dot{\hat{x}}(t) = A_m \hat{x}(t) + B_m\Big(\hat{\omega}(t)u_a(t) + \hat{\theta}(t)\|x(t)\|_{\mathcal{L}_\infty} + \hat{\sigma}(t)\Big) \tag{28}$$

- Adaptation Phase: This stage uses the error between the measured states and the estimated ones to adapt the parameters while considering a projection method in order to ensure their boundedness. In fact, a projection operator avoids the parameter drift using the gradient of a convex function and a maximal bound on the parameters to be estimated. The adapation law for

each estimated parameter is given by:

$$\begin{aligned}\dot{\hat{\theta}}(t) &= \Gamma Proj(\hat{\theta}(t), -(\tilde{x}^T(t)PB_m)^T \|x(t)\|_{\mathcal{L}_\infty}) \\ \dot{\hat{\sigma}}(t) &= \Gamma Proj(\hat{\sigma}(t), -(\tilde{x}^T(t)PB_m)^T) \\ \dot{\hat{\omega}}(t) &= \Gamma Proj(\hat{\omega}(t), -(\tilde{x}^T(t)PB_m)^T u_a^T(t))\end{aligned} \tag{29}$$

The parameter P is the solution to the algebraic Lyapunov equation: $A_m^T P + PA_m^T = -Q$ for any arbitrary symmetric matrix $Q = Q^T > 0$. Γ is the adaptation gain and $\tilde{x}(t)$ the prediction error.

- Control law formulation: The last stage pertains to the formulation of the control input characterized by the addition of a low pass filter. It is written as:

$$u_a(s) = -kD(s)(\hat{\eta}_l(s) - k_g r) \tag{30}$$

$D(s)$ is an $m \times m$ strictly proper transfer function leading to the stable closed-loop filter: $C(s) = \frac{\omega k D(s)}{\mathbb{I}_m + \omega k D(s)}$. k is a positive feedback gain, $k_g = -(CA_m^{-1}B_m)^{-1}$ is a feedforward prefilter applied to the reference signal $r(t)$ and $\hat{\eta}_l = \hat{\omega}(t)u_a(t) + \hat{\theta}\|x(t)\|_{\mathcal{L}_\infty}$. To ensure the stability of the closed-loop system, the feedback gain k and the filter $D(s)$ must be chosen in order to fulfill the $\mathcal{L}_1$ norm condition. The reader can refer to (Hovakimyan & Cao, 2010) for a detailed proof of stability.

This control architecture with the equations included can be summarized in Figure 3.

3.2.2. Application to the studied dynamics

This control architecture is applied on two degrees of freedom: the depth z and the pitch ϑ of our underwater vehicle. Combining (8), (25) and (26) we get the full dynamics in the earth frame to be:

$$\begin{bmatrix} \dot{\eta}_1 \\ \dot{\eta}_2 \end{bmatrix} = \begin{bmatrix} 0_{2\times2} & \mathbb{I}_2 \\ 0_{2\times2} & \frac{-D_r^*}{M_r^*} \end{bmatrix} \begin{bmatrix} \eta_1 \\ \eta_2 \end{bmatrix} - \begin{bmatrix} 0_{2\times1} \\ \frac{g_r^*}{M_r^*} - \frac{w_{d_r}^*}{M_r^*} \end{bmatrix} + \begin{bmatrix} 0_{2\times2} \\ \frac{1}{M_r^*} \end{bmatrix} \omega\tau_r^* \tag{31}$$

with $\eta_1 = [z\ \vartheta]^T$ and $\eta_2 = [\dot{z}, \dot{\vartheta}]^T$. In this case $\omega \in \mathbb{R}^{2\times2}$ is considered to be an identity matrix. Rewriting (31) in the form of (28) in terms of the state matrix A_m and the parameters ω, θ and σ, we get:

$$\begin{bmatrix} \dot{\eta}_1 \\ \dot{\eta}_2 \end{bmatrix} = A_m \begin{bmatrix} \eta_1 \\ \eta_2 \end{bmatrix} + \begin{bmatrix} 0_{2\times2} \\ \frac{1}{M_r^*} \end{bmatrix} (\omega u_a + \theta(t)\|\eta(t)\|_{\mathcal{L}_\infty} + \sigma(t)) \tag{32}$$

$$y = \begin{bmatrix} 1 & 0 & 0 & 0 \\ 0 & 1 & 0 & 0 \end{bmatrix} \begin{bmatrix} \eta_1 \\ \eta_2 \end{bmatrix} = \begin{bmatrix} z \\ \vartheta \end{bmatrix} \tag{33}$$

where A_m is obtained from a choice of k_m rendering the state matrix Hurwitz, with $A_m \in \mathbb{R}^{4\times4}$ and $B_m = [0_{2\times2}, \frac{1}{M_r^*}]^T \in \mathbb{R}^{4\times2}$. The parameters' vector $\theta \in \mathbb{R}^2$ includes the uncertainties on the damping coefficients and is given by: $\theta = \left[\Delta(-D_z^*)\,,\ \Delta(-D_\vartheta^*)\right]^T$. The parameter $\sigma \in \mathbb{R}^2$ is a lumped parameter regrouping the gravitational and buoyancy forces as well as the external disturbances $\sigma = \left[-g_z^* + w_{d_z}^*\,,\ -g_\vartheta^* + w_{d_\vartheta}^*\right]^T$. The parameter $\omega \in \mathbb{R}^{2\times2}$ is considered constant and will not be adapted for this study as we have a precise knowledge of the

motors' features. The expression $\|\eta(t)\|_{\mathcal{L}_\infty}$ refers to the infinity norm of the state vector η at instant t. As shown in equation (33), the outputs of the system are z and ϑ. The control input is computed in the earth fixed frame and consequently should be transformed into the body fixed frame. The system's control input is computed as follows: $u = K^{-1}T^{-1}J^T(u_a + u_m) \in \mathbb{R}^2$, with u_a and u_m as explained above.

Remark 1: In the matrices A_2 and B_2, the elements M_z^*, M_ϑ^* and D_z^*, D_ϑ^* are likely to vary since they depend on the orientation of the vehicle given that they are computed in the earth frame. We have mentioned before that A_m and B_m should be constant and for the sake of consistency, we replace these starred model elements with M_z, M_ϑ, D_z and D_ϑ. This will guarantee for A_m a constant desired dynamics. All the uncertainties will be compensated in the vectors of the controlled parameters $\hat{\theta}$ and $\hat{\sigma}$ that are to be adapted. It has to be noticed that unlike for the ANSF, no *a priori* knowledge of these parameters is required and they have been initialized to zero.

4. Experimental testbed

The AC-ROV submarine (cf. Figure 4) is an underactuated vehicle. Its propulsion system consists of six thrusters driven by DC motors and controlling five degrees of freedom. The motors $1, 2, 3$ and 4 control simultaneously translations along x and y axes and rotation around the z axis (yaw angle). Motors 5 and 6 control depth and pitch. Roll is left uncontrolled but remains naturally stable due to the

Table 1: Parameters' values of the ANSF controller used in the experiments.

Parameter	Description	Value	Parameter	Description	Value
c_o	Constant gain	0.1	K_{P_z}	Proportional gain of z	0.42
c_1	Constant gain	0.05	K_{I_z}	Integral gain of z	0.055
$M_{z_{initial}}$	Initial value of mass of z	1 kg	K_{D_z}	Derivative gain of z	0.05
$D_{z_{initial}}$	Initial value of damping of z	0.2 N.s/m	K_{P_ϑ}	Proportional gain of ϑ	0.2
$M_{\vartheta_{initial}}$	Initial value of mass of ϑ	0.117 kg.m	K_{I_ϑ}	Integral gain of ϑ	0.055
$D_{\vartheta_{initial}}$	Initial value of mass of damping of ϑ	0.01 N.s/m	K_{D_ϑ}	Derivative gain of ϑ	0.05
$(W-B)_{initial}$	Initial value of the floatability	0.7 N	Γ_z	Adaptation gain of z	0.2
$z_G W_{initial}$	Initial value of the restoring torque of ϑ	0.055 N.m	Γ_ϑ	Adaptation gain of ϑ	1

Table 2: Parameters' values of the $\mathcal{L}_1$ adaptive controller used in the experiments.

Parameter	Description	Value	Parameter	Description	Value
$\sigma_{z_{initial}}$	Initial value for the nonlinear parameter of z	0	k_z	Feedback gain of z	0.4
$\sigma_{\vartheta_{initial}}$	Initial value for the nonlinear parameter of ϑ	0	k_ϑ	Feedback gain of ϑ	0.3
$\theta_{z_{initial}}$	Initial value for the parameter θ of z	0	Γ_z	Adaptation gain of z	10000
$\theta_{\vartheta_{initial}}$	Initial value for the parameter θ of ϑ	0	Γ_ϑ	Adaptation gain of ϑ	1300

relative position of buoyancy and gravity centers. The robot weighs 3 *kg* and has a rectangular shape with height 203 *mm*, length 152 *mm* and width 146 *mm*. For measurement purposes, the prototype is equipped with different sensors. A 6-DOF IMU (Inertial Measurement Unit) measures roll, pitch, and yaw along with their respective velocities. A pressure sensor is used for depth measurement. Once the control law has been computed by the control PC, the control inputs are transmitted to the power stage. Then, six PWM modulated signals are sent to the motors of the AC-ROV through a 40-meter long tether. Figure 4-(b) shows a schematic view summarizing the various components of the system's hardware

and their interactions.

The real-time experiments have been performed in a 5 m^3 pool. The tether has been sufficiently deployed to avoid inducing additional drag into the dynamics of the vehicle. The feedback gains have been tuned for the nominal conditions and kept unchanged for the rest of the experimental scenarios despite the eventual changes in the model or its environment in order to evaluate the robustness of the proposed controller. The information concerning the velocity in the z direction is estimated by an alpha-beta observer.

5. Real-time experimental results

In this section, the obtained experimental results are presented and discussed. They result from the application of the controllers detailed in section III to the underwater vehicle testbed described in section IV. The different performed scenarios are explained and then the obtained results are presented through Figures 5 to 10 and analyzed. The considered initial position of the vehicle is the surface (horizontal static position) then it is controlled to reach a depth of 0.8 m and a pitch angle of 10 deg. In fact, the tested trajectories (in pitch and depth) have been chosen so as to avoid thrusters' saturation (i.e a maximum force of 1 N) and that is why the desired depth and pitch are reached within 40 seconds and the pitch is limited to 10 deg. It is worth to note that these results can easily be extended to larger scale and faster trajectories in case of more powerful actuators. For each experimental scenario, the evolution of the control inputs, generated by thrusters 5 and 6 (cf. Figure 4-(a)) controlling these two degrees of freedom as well as the

evolution of the estimated parameters are plotted. Only parameters pertaining to gravity and buoyancy are retained for the ANSF controller since they are the ones with a great impact on the dynamical model. The other parameters did not vary enough and therefore are not displayed. Tables 1 and 2 summarizes the values of all the parameters and gains used in these experiments.
The reader can refer to the following internet link for a video with experimental results: www.lirmm.fr/~creuze/ocean/

5.1. Proposed Experimental Scenarios

Three experimental scenarios were performed, namely:

i) *Scenario 1*: *Control in nominal conditions*

The objective of this scenario is to control the depth of the AC-ROV without considering any external disturbances. The gains for each controller have been tuned (cf. Tables 1 and 2 to accomodate this case and were kept unchanged for the rest of the experiments.

ii) *Scenario 2: Punctual external disturbance rejection*

In this scenario, when the robot reached its steady state position, an external punctual disturbance was applied by giving the robot a quick kick pushing it downwards. The objective of this experiment is to see whether the controllers are able to drive the system back to its regulated position. Such a situation corresponds to the case where the vehicle hits a rock or an underwater structure, or collides with another vehicle or floating obstacle.

iii) *Scenario 3: Robustness towards parameter uncertainty*

The model of the vehicle was changed right before starting this scenario by the addition of a rectangular piece of polyester introducing then a change of buoyancy of $+0.2\ N$ and bringing a variation of approximately 15% with respect to the minimal value of the parameter $(W - B)$. Such a variation corresponds for instance to the situation where the vehicle encounters a sudden change in the water's salinity.

5.2. Control in nominal conditions

Figures 5 and 6 display the evolution of the vehicle's position for each of the proposed controllers. The robot is expected to follow a trajectory in depth going from the surface and reaching $0.8\ m$ in $40\ s$ and another one in pitch going from $0\ deg$ at t=100 s and reaching $\vartheta = 10\ deg$ in $40\ s$. The ANSF controller in Figures 5-(a) needs around $85\ s$ to reach the steady state depth (5% of the final value) with no significant overshoot. The desired pitch of the same controller was reached much faster ($\simeq 65\ s$) with no significant overshoot either. The $\mathcal{L}_1$ adaptive controller reveals to have a similar convergence slope for the depth but remains slightly faster with $75\ s$ while the pitch angle was able to follow the desired trajectory. Both degrees of freedom do not exhibit any overshoot. The similarity in the responses of these two controllers is seen through the root mean square errors (cf. Table 3), but we can still deduce that the $\mathcal{L}_1$ adaptive controller was faster and this is due to the better trajectory following achieved. We observe that for both controllers we have a smooth response of the thrusters that exert a total force of $1.25\ N$ (cf. Figures 5-(b), 6-(b)) as well as a parameter convergence to steady state values

(cf. Figures 5-(c), 6-(c)). On the latter two figures we observe that the parameters of the ANSF were initialized with a rough knowledge of the system. Moreover, small adaptation gains have been used in order to converge easily to a suitable set of parameters. The controlled parameters of the $\mathcal{L}_1$ adaptive controller were all initialized to zero and although the adaptation gains were very high a smooth convergence is observed. We conclude from this scenario that the $\mathcal{L}_1$ adaptive controller is able to ensure a faster output convergence without the necessity of having any *a priori* knowledge of the model parameters. It has to be noticed that regardless of the considered controller, the pitch angle shows some oscillations during the first 40 s. This behavior is due to the fact that the vehicle starts its trajectory from the surface, thus leading to disturbances that cannot be compensated since the propellers are not fully immersed during this initial period of time.

5.3. Punctual external disturbance rejection

As specified earlier, an external punctual disturbance has been applied on the vehicle after it reached the steady state position (cf. Figures 7, 8. Due to the experimental setup of this scenario, the desired pitch angle was set to 0. The disturbance was applied at time $t = 245$ s to cause a positive depth error of 15 cm. The recovery time was of 15 s for the ANSF controller against 10 s for the $\mathcal{L}_1$ adaptive controller. A small overshoot can be noticed with the $\mathcal{L}_1$ adaptive controller for the depth whereas the ANSF converged with no overshoot but a static error of about 5 cm is conserved for 30 s; the pitch angle for this controller was more severely affected by this disturbance but it was also able to stabilize again in 15 s.

The root mean square errors in this scenario favours the ANSF controller for the pitch since it maintained its stable position more accurately whereas the depth was better compensated with the $\mathcal{L}_1$ adaptive controller. These differences in the system's response of each controller are also reflected in Figures 7-(b) and 8-(b) where the control input of the $\mathcal{L}_1$ adaptive controller is seen to react smoothly with a more significant change in its estimated parameters as seen in Figure 8-(c).

5.4. Robustness towards parameter uncertainty

The additional buoyancy added to the system disturbs in a persistant way the motion of the vehicle that would tend to float more. The depth response of the ANSF is seen to have a delay of 10 s compared to the nominal case (cf. Figure 9) furthermore the slope of the response of this degree of freedom was attenuated at the middle of the trajectory due to the additional time needed for a complete parameter convergence of the parameter $(W - B)$ as seen in Figure 9-(c). This parameter influencing greatly the dynamics in depth converged to -1.1 N in this scenario compared to -0.95 N in the nominal case. This parameter is the most dominant one for the dynamics studied. The pitch angle's convergence time was delayed by 20 s and the parameter $z_G W$ showed a change from 0.035 mN to 0.015 mN, since the position of the center of buoyancy is the center of our frame of reference and it gets modified with this added persistent disturbance. On the contrary, when the $\mathcal{L}_1$ adaptive controller was applied, the system reponse times for both degrees of freedom were kept unchanged. However, we observed a stronger level of noise in the response of the pitch angle. The differences in the root mean square errors

between the controllers are significant on the depth compared to the nominal case. Given that no static erros are observed at steady state, this shows how the system was slowed down with the ANSF. As for the depth, the residual oscillations made the RMSE for this degree of freedom not very relevant after the average was made for both controllers. The fact that no additional delays were observed for the $\mathcal{L}_1$ adaptive controller despite the added buoyancy, can be explained by its fast adaptation that guarantees the convergence of the parameters to their new values. (In the nominal case we had $\hat{\theta} = [7, -26]^T$ and $\hat{\sigma} = [10, -100]^T$ becoming $\hat{\theta} = [6, -22]^T$ and $\hat{\sigma} = [12, -135]^T$ with added buoyancy). As stated in (Slotine & Weiping, 1991), It is worth to note that adaptative controllers do not necessarly ensure the convergence of the updated parameters to their desired values to obtain the convergence of the system to its desired position. The control law itself (13) in the case of the ANSF controller, and the parameter projection (29) in the case of the $\mathcal{L}_1$ adaptive controller ensure the boundedness of the parameters but not necessarily their convergence to the real values. The control inputs generated by both controllers, are depicted in Figures 9-(b) and 10-(b). Compared to the nominal case, we can observe that the robot's actuators are exerting more effort in order to immerse the vehicle while keeping the desired pitch angle; we have a combined force of 1.45 N compared to 1.25 N in the nominal case.

6. Comparison study of the proposed adaptive control schemes

Table 3 below summarizes in a quantitative manner the comparisons performed above between the two proposed controllers for the different proposed experimen-

tal scenarios. Some relevant criteria have been chosen to perform this comparison. Indeed, throughout the performed experiments, it was noticed that the $\mathcal{L}_1$ adaptive controller drived the system faster to the desired state due to the decoupling aspect between robustness and adaptation. On the contrary, the adaptation gains of the ANSF controller had to be chosen relatively small in order to avoid oscillating responses and even instability of the system. For this reason, we found important discrepancies among both controllers' behaviors when a parameter of the model was modified. Both showed to be robust to this persistant disturbance but the ANSF controller needs more time to overcome this variation while no significant difference compared to the nominal case was observed with the $\mathcal{L}_1$ adaptive controller. For this reason, the latter controller reacted also faster in presence of an external disturbance and therefore recovered faster. An important point to be reminded concerns the initialization of the parameters' vector to be estimated for each controller. The ANSF controller's parameters need to be initialzed with some suitable values requiring a sufficient knowledge of the system while the parameters of the $\mathcal{L}_1$ adaptive controller can be initialized to 0.

7. Conclusion and Future Work

This paper deals with control of an underwater vehicle considering the challenges arising from the high nonlinearities of the system's dynamics and the variations of its parameters. The proposed solution includes the design and real-time implementation of an $\mathcal{L}_1$ adaptive controller known by its particular architecture where robustness and adaptation are decoupled. To the best knowledge of the authors,

Table 3: Controllers Performance Comparison

Nominal Conditions	**ANSF**		**$\mathcal{L}_1$ Controller**	
	z	ϑ	z	ϑ
Settling Time	85 *s*	65 *s*	75 *s*	40 *s*
Maximum Overshoot	0%	0%	0%	0%
Root Mean Square Error	25.3 *cm*	5.6 *deg*	24.4 *cm*	5.1 *deg*
Punctual Disturbance				
	z	ϑ	z	ϑ
Recovery Time	15 *s*	15 *s*	10 *s*	10 *s*
Maximum Overshoot	0%	50%	6%	50%
Root Mean Square Error	5.8 *cm*	0.6 *deg*	2.7 *cm*	1.5 *deg*
Change in Buoyancy				
	z	ϑ	z	ϑ
Settling Time	95 *s*	85 *s*	75 *s*	40 *s*
Maximum Overshoot	0%	0%	0%	0%
Root Mean Square Error	30.1 *cm*	5.3 *deg*	26.1 *cm*	5.3 *deg*

this is the first study evaluating the performance of such a controller on an underwater vehicle. Indeed, to highlight the advantages of this controller it was experimentally compared with the well proven ANSF controller. Various scenarios are proposed to evaluate the closed-loop system behavior in nominal conditions as well as in presence of parameters' changes and external disturbances. This study showed that both controllers are capable of compensating the introduced uncertainties and external disturbances. However, the $\mathcal{L}_1$ adaptive controller was faster in adaptation despite the zero initialization of its parameters. Future work could involve the modeling of the thrusters's dynamics and their incorporation in the

controlled system.

References

Antonelli, G. 2003. A New Adaptive Control Law for the Phantom ROV. Pages 569–574 of: 7th IFAC Symposium on Robot Control.

Antonelli, G. 2007. On the use of Adaptive/Integral actions for Six-Degrees-of-Freedom control of Autonomous Underwater Vehicles. IEEE Journal of Oceanic Engineering, **32**(Apr.), 300–312.

Antonelli, G., Chiaverini, S., Sarkar, N., & West, M. 1999. Adaptive control of an autonomous underwater vehicle: experimental results on ODIN. Pages 64–69 of: Proceedings IEEE International Symposium on Computational Intelligence in Robotics and Automation CIRA'99.

Antonelli, G., Cacciavale, F., Chiaverini, S., & Fusco, G. 2001. A novel adaptive control law for Autonomous Underwater Vehicle. Pages 447–452 of: Proceedings of the IEEE International Conference on Robotics and Automation ICRA'01.

Antonelli, Gianluca. 2006. An Adaptive Law for Guidance and Control of Remotely Operated Vehicles. Pages 1–6 of: 14th Mediterranean Conference on Control and Automation MED'06.

Cao, Chenguy, & Hovakimyan, Naira. 2008. $\mathcal{L}_1$ adaptive controller for nonlinear

systems in the presence of unmodelled dynamics: Part II. American Control Conference, Seattle, WA.

Carreras, M., Yuh, J., & JBatlle, J. 2002. High-Level control of autonomous robots using a behavior-based scheme and reinforcement learning. In: 15th Triennial World Congress of the International Federation of Automatic Control.

Chang, M., Chang, W., & Liu, H.H. 2003. Model-Based fuzzy modeling and control for autonomous underwater vehicles in the horizontal plane. Journal of Marine Sciences and Technology, **11**, 155–163.

Dobrokhodov, V.N., Xargay, E, Hovakimyan, N, Kaminer, I.I., Kitsios, I, Cao, C, Gregory, I, & Valavani, L. 2010. Experimental Validation of $\mathcal{L}_1$ Adaptive Control: Rohrs' Counterexample in Flight. Journal of Guidance, Control, and Dynamics,.

Fan, X, & Smith, R.C. 2008. $\mathcal{L}_1$ adaptive control of hysteresis in smart materials. Proceedings of the SPIE Smart Structures/NDE, 15th Annual International Symposium, San Diego, CA.

Fjellstad, O.-E., & Fossen, T.I. 1994a. Singularity-free tracking of unmanned underwater vehicles in 6 DOF. Pages 1128–1133 of: Proceedings of the 33rd IEEE Conference on Decision and Control. Florida, USA: IEEE.

Fjellstad, O.E, & Fossen, T.I. 1994b. Position and attitude tracking of AUV's: A quaternion approach. IEEE Journal of Ocean Engineering, **19**(4), 512–518.

Fossen, Thor I., & Fjellstad, Ola-Erik. 1996. Robust adaptive control of underwater vehicles: A comparative study. Pages 47–61 of: IFAC Workshop on Control Applications in Marine Systems (CAMS'95) No3,, vol. 17. Trondheim, Norway: Research Council of Norway, Oslo.

Fossen, T.I. 2002. Marine Control Systems:Guidance, Navigation and Control of Ships, Rigs and Underwater Vehicles. As,Trondheim: Marine Cybernetics.

Fossen, T.I, & Balchen, J. 1991 (Oct). The NEROV autonomous underwater vehicle. Proceedings of the OCEANS conference, Honolulu, HI.

Fossen, T.I., & Sagatun, S.I. 1991 (April). Adaptive control of nonlinear underwater robotic systems. Pages 1687–1695 of: Proceedings of the IEEE International Conference on Robotic and Automation ICRA'91.

Hovakimyan, N, & Cao, C. 2010. $\mathcal{L}_1$ Adaptive Control Theory. Society of Industrial and Applied Mathematics.

Kaminer, I, Pascoal, A, Xargay, E, Cao, C, & Dobrokhodov, V. 2010. Path following for unmanned aerial vehicles using $\mathcal{L}_1$ adaptive augmentation of commercial autopilots. Journal of Guidance, Control and Dynamics, **33**(2).

Kim, T.W., & Yuh, J. 2001. A novel neuro-fuzzy controller for autonomous underwater vehicles. Pages 2350–2355 of: Proceedings of the IEEE International Conference on Robotics and Automation ICRA'99, vol. 4.

Lapierre, Lionel. 2009. Robust diving control of an AUV. Ocean Engineering, **36**(November), 92–104.

Lapierre, Lionel, & Soetanto, Didik. 2007. Nonlinear path-following control of an AUV. Ocean Engineering, **34**, 1734–1744.

Maalouf, Divine, Creuze, Vincent, & Chemori, Ahmed. 2012 (Oct). A novel application of multivariable l1 adaptive control: From design to real-time implementation on an underwater vehicle. IEEE/RSJ IROS'12, Algarve, Portugal.

Marzbanrad, A.R, Eghtesad, M, & Kamali, R. 2011. A Robust Adaptive FUzzy Sliding Mode Controller for Trajectory Tracking of ROVs. Pages 2863–2869 of: 50th IEEE Conference onf Decision and Control and European Control Conference (CDC-ECC).

Narendra, K, & Annaswamy, A.M. 1987. A new adaptive law for robust adaptation without persistent excitation. IEEE Transactions on Automatic Control, **32**, 134–145.

Pisano, Alessandro, & Usai, Elio. 2004. Output-feedback control of an underwater vehicle prototype by higher-order sliding modes. Automatica, **40**(9), 1525–1531.

Roche, Emilie, Sename, Olivier, Simon, Daniel, & Varrier, S. 2011. A Hierarchical Varying Sampling $\mathcal{H}_\infty$ Control of an AUV. In: 18th IFAC world congress.

Rohrs, C.E, Valavani, L, Athans, M, & Stein, G. 1982 (December). Stability problems of adaptive control algorithms in the presence of unmodeled dynamics. 21st Conference on Decision and Control, Orlando,FL.

Sadegh, N., & Horowitz, R. 1990. Stability and robustness analysis of a class of adaptive controllers. Robustness analysis of a class of adaptive controllers for robotic manipulators, **35**, 74–94.

Slotine, J.J, & Weiping, Li. 1991. Applied Nonlinear Control. Englewoods Cliffs, New Jersey: Prentice-Hall Int.

Slotine, J.J.E, & Benedetto, M.D.Di. 1990. Hamiltonian adaptive control of spacecraft. IEEE Transactions on Automatic Control, **35**(7), 848–852.

Steenson, Leo V, Phillips, Alexander B., Rogers, Eric, Furlong, Maaten E., & Turnock, Stephen R. 2012 (April). Experimental Verification of a Depth Controller using Model Predictive Control with Constraints onboard a Thruster Actuated AUV. IFAC Workshop on Navigation, Guidance and Control of Underwater Vehicles (NGCUV2012), Ireland.

Sun, Y.C, & Chea, C.C. 2003 (December). Adaptive Setpoint for Autonomous Underwater Vehicles. Proceedings of the 42nd IEEE Conference on Decision and Control, Maui,Hawaii.

Techy, L, Reddy, C.K, Woolsey, C A, Cao, C, & Hovakimyan, N. 2007 (July). Nonlinear Control of a Novel Two-Link Pendulum. American Control Conference, New York City,USA.

Yildiz, O., Yilma, A.E., & Gokalp, B. 2009. State-of-the-Art System Solutions for Unmanned Underwater Vehicles. Radioengineering, **18**(4), 590–600.

Yuh, J. 2000. Design and Control of Autonomous Underwater Robots : A Survey. Autonomous Robots, **24**, 7–24.

Yuh, J, Nie, J, & Lee, C.S.G. 1999 (May). Experimental Study on Adaptive Control of Underwater Robots. Proceedings of The IEEE International Conference on Robotics and Automation, Michigan, USA.

Yuh, Junky, & Nie, Jing. 2000. Application of non-regressor-based adaptive control to underwater robots: experiment. Computers and Electrical Engineering, **26**(February), 169–179.

Zang, Z, & Bitmead, R.R. 1990. Transient bounds for adaptive control systems. IEEE Conference on Decision and Control.

Zhao, Side, & Yuh, Junku. 2000. Experimental Sutdy on Advanced Underwater Robot Control. IEEE Transactions on Robotics, **21**(4), 695–703.

Figure

Figure 1: View of the AC-ROV and its reference frames ($x_i y_i z_i$: earth-fixed frame, $x_b y_b z_b$: body-fixed frame).
Figure 2: Block diagram of the closed-loop $\mathcal{L}_1$ adaptive controller.
Figure 3: Detailed block-diagram of the $\mathcal{L}_1$ adaptive control architecture.
Figure 4: (a): Description of the AC-ROV and its components, (b): Schematic view of its hardware architecture.
Figure 5: **ANSF controller (control in nominal case):** (a) the system outputs' responses (z and ϑ), (b) the control inputs, and (c) the estimated parameters $\widehat{M}_r$ and $\hat{g}_r$.
Figure 5-(a): Time history of the measured depth position z and pitch angle ϑ as well as their respective desired trajectories.
Figure 5-(b): Time history of the force generated by the two thrusters controlling z and ϑ.
Figure 5-(c): Time history of the evolution of the parameters $\widehat{M}_r = [\widehat{M}_z \ \widehat{M}_\vartheta]^T$ and $\hat{g}_r = [\widehat{W-B} \ \widehat{z_G W}]^T$.
Figure 6: **$\mathcal{L}_1$ Adaptive Controller (control in nominal case):** (a) the system outputs' responses (z and ϑ), (b) the control inputs, and (c) the estimated parameters $\hat{\theta}$ and $\hat{\sigma}$ (c).
Figure 6-(a): Time history of the measured depth position z and pitch angle ϑ as well as their respective desired trajectories.
Figure 6-(b): Time history of the force generated by the two thrusters controlling z and ϑ.
Figure 6-(c): Time history of the evolution of the parameters $\hat{\theta} = [\hat{\theta}_z \ \hat{\theta}_\vartheta]^T$ and the nonlinear terms $\hat{\sigma} = [\hat{\sigma}_z \ \hat{\sigma}_\vartheta]^T$.
Figure 7: **ANSF Controller (punctual external disturbance rejection):** (a) the system outputs' responses (z and ϑ), (b) the control inputs, and (c) the estimated parameters $\widehat{M}_r$ and $\hat{g}_r$.
Figure 7-(a): Time history of the measured depth position z and pitch angle ϑ as well as their respective desired trajectories.
Figure 7-(b): Time history of the force generated by the two thrusters controlling z and ϑ.
Figure 7-(c): Time history of the evolution of the parameters $\widehat{M}_r = [\widehat{M}_z \ \widehat{M}_\vartheta]^T$ and $\hat{g}_r = [\widehat{W-B} \ \widehat{z_G W}]^T$.
Figure 8: **$\mathcal{L}_1$ Adaptive Controller (punctual external disturbance rejection):** (a) the system outputs' responses (z and ϑ), (b) the control inputs, and (c) the estimated parameters $\hat{\theta}$ and $\hat{\sigma}$.
Figure 8-(a): Time history of the measured depth position z and pitch angle ϑ as well as their respective desired trajectories.
Figure 8-(b): Time history of the force generated by the two thrusters controlling z and ϑ.
Figure 8-(c): Time history of the evolution of the parameters $\hat{\theta} = [\hat{\theta}_z \ \hat{\theta}_\vartheta]^T$ and the nonlinear terms $\hat{\sigma} = [\hat{\sigma}_z \ \hat{\sigma}_\vartheta]^T$.
Figure 9: **ANSF Controller (robustness towards parameter uncertainty):** (a)

the system outputs' responses (z and ϑ) are slower than those observed in the nominal case. The change of buoyancy is observed through the plots of the control inputs (b) and the estimated parameters $\widehat{M}_r$ and $\hat{g}_r$ (c).
Figure 9-(a): Time history of the measured depth position z and pitch angle ϑ as well as their respective desired trajectories.
Figure 9-(b): Time history of the force generated by the two thrusters controlling z and ϑ.
Figure 9-(c): Time history of the evolution of the parameters $\widehat{M}_r = [\widehat{M}_z \ \widehat{M}_\vartheta]^T$ and $\hat{g}_r = [\widehat{W-B} \ \widehat{z_G W}]^T$.
Figure 10: **$\mathcal{L}_1$ Adaptive Controller (robustness towards parameter uncertainty):** (a) the system outputs' responses (z and ϑ) have the same convergence rate as the one in the nominal case. The change of buoyancy is observed through the plots of the control inputs (b) and the estimated parameters (c).
Figure 10-(a): Time history of the measured depth position z and pitch angle ϑ as well as their respective desired trajectories.
Figure 10-(b): Time history of the force generated by the two thrusters controlling z and ϑ.
Figure 10-(c): Time history of the evolution of the parameters$\hat{\theta} = [\hat{\theta}_z \ \hat{\theta}_\vartheta]^T$ and the nonlinear terms $\hat{\sigma} = [\hat{\sigma}_z \ \hat{\sigma}_\vartheta]^T$.

Figure

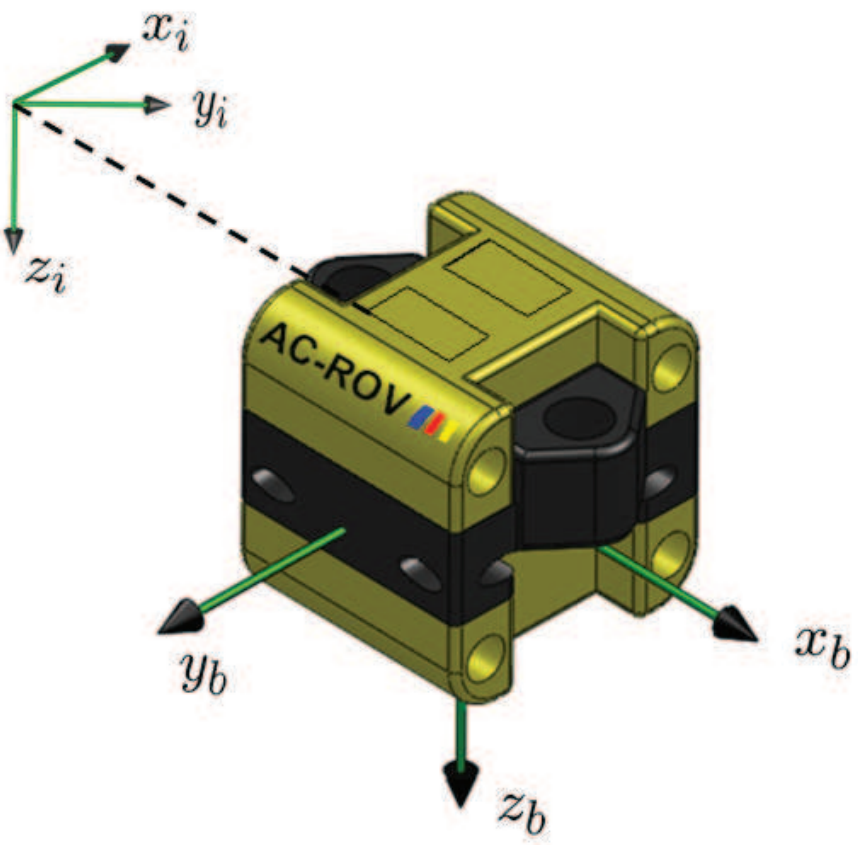

Figure

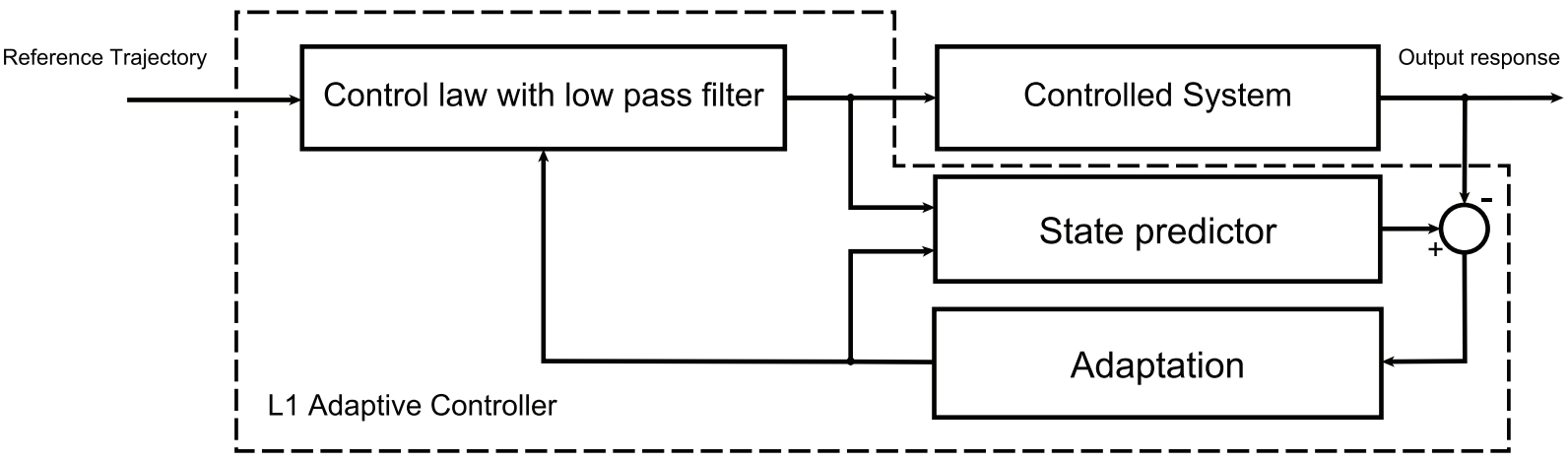
Reference Trajectory
Control law with low pass filter
Controlled System
Output response
State predictor
-
+
Adaptation
L1 Adaptive Controller

Figure

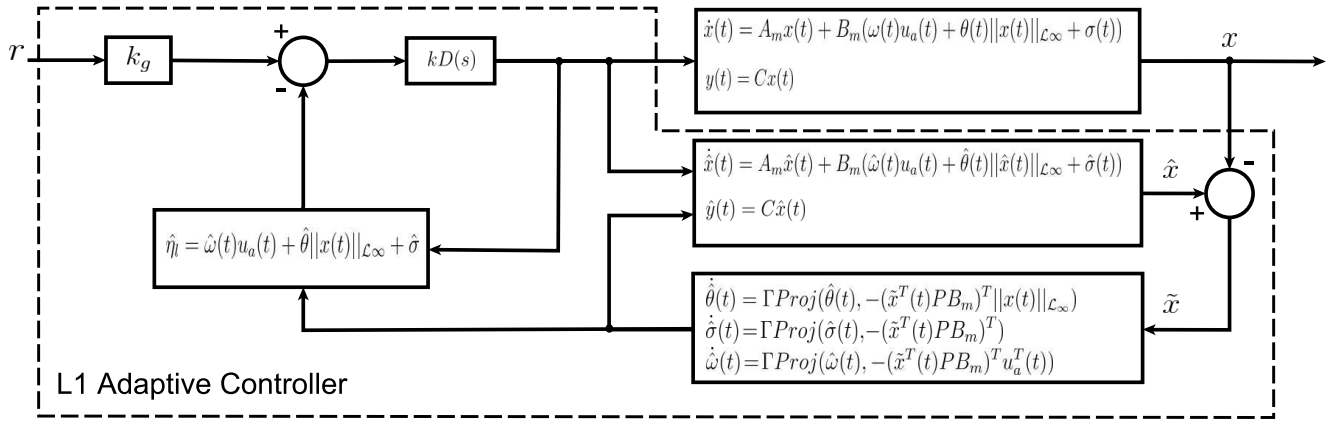
r
k_g
+
-
$kD(s)$
$\dot{x}(t) = A_m x(t) + B_m(\omega(t)u_a(t) + \theta(t)||x(t)||_{\mathcal{L}\infty} + \sigma(t))$
$y(t) = Cx(t)$
x
$\dot{\hat{x}}(t) = A_m\hat{x}(t) + B_m(\hat{\omega}(t)u_a(t) + \hat{\theta}(t)||\hat{x}(t)||_{\mathcal{L}\infty} + \hat{\sigma}(t))$
$\hat{y}(t) = C\hat{x}(t)$
$\hat{x}$
+
-
$\hat{\eta}_l = \hat{\omega}(t)u_a(t) + \hat{\theta}||x(t)||_{\mathcal{L}\infty} + \hat{\sigma}$
$\dot{\hat{\theta}}(t) = \Gamma Proj(\hat{\theta}(t), -(\tilde{x}^T(t)PB_m)^T||x(t)||_{\mathcal{L}\infty})$
$\dot{\hat{\sigma}}(t) = \Gamma Proj(\hat{\sigma}(t), -(\tilde{x}^T(t)PB_m)^T)$
$\dot{\hat{\omega}}(t) = \Gamma Proj(\hat{\omega}(t), -(\tilde{x}^T(t)PB_m)^T u_a^T(t))$
$\tilde{x}$
L1 Adaptive Controller

Figure

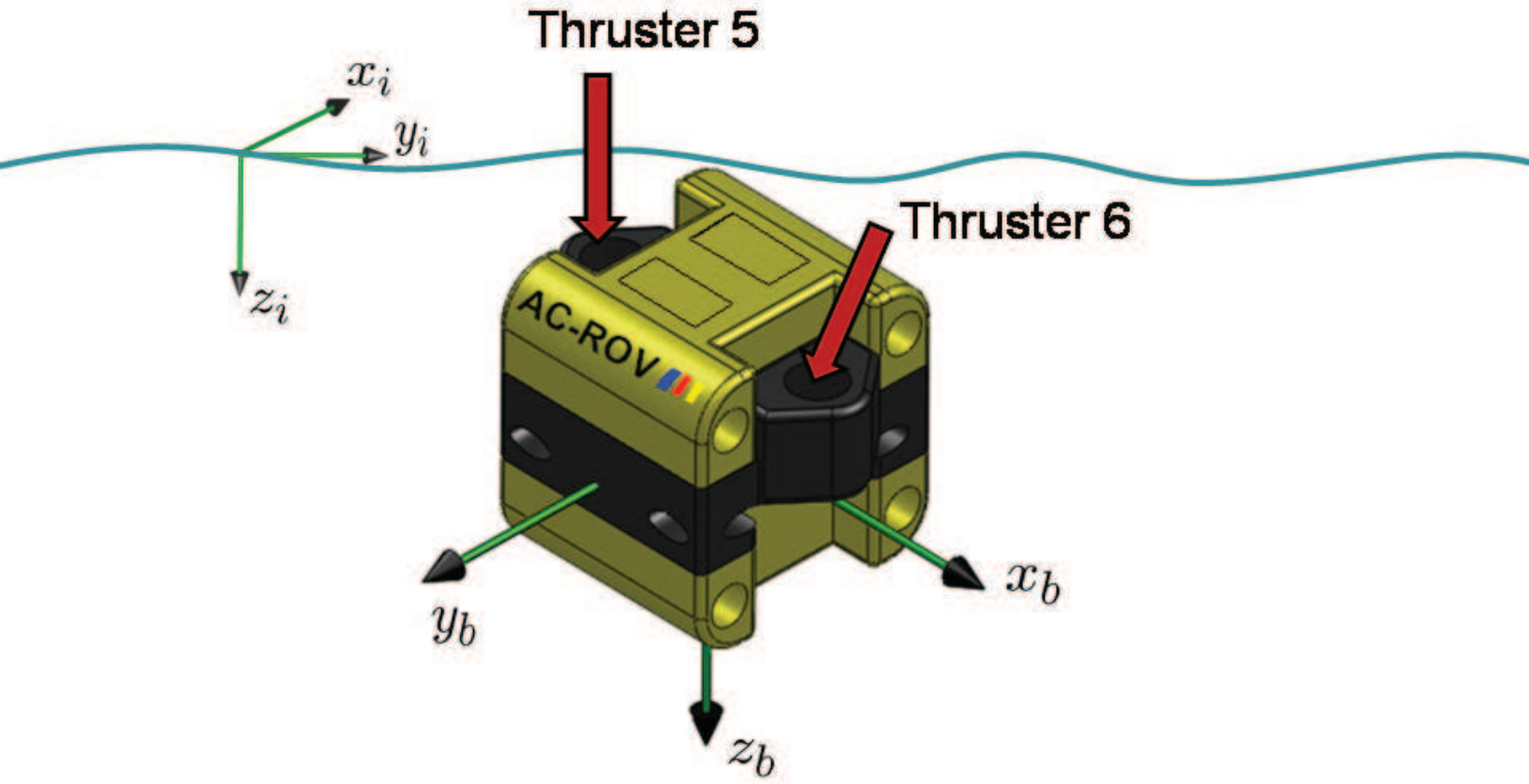

Figure

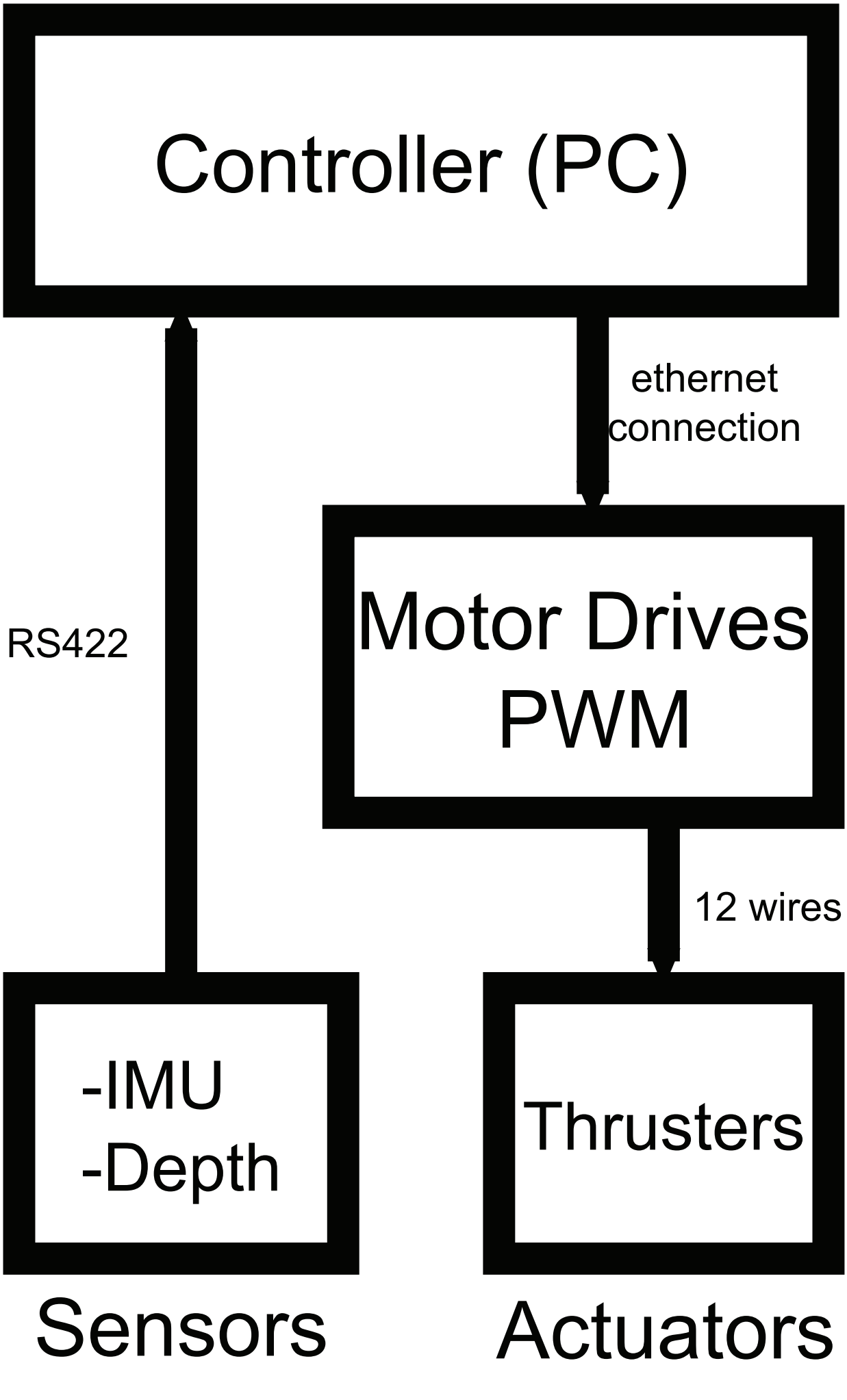
Controller (PC)
ethernet
connection
RS422
Motor Drives
PWM
12 wires
-IMU
-Depth
Thrusters
Sensors
Actuators

Figure

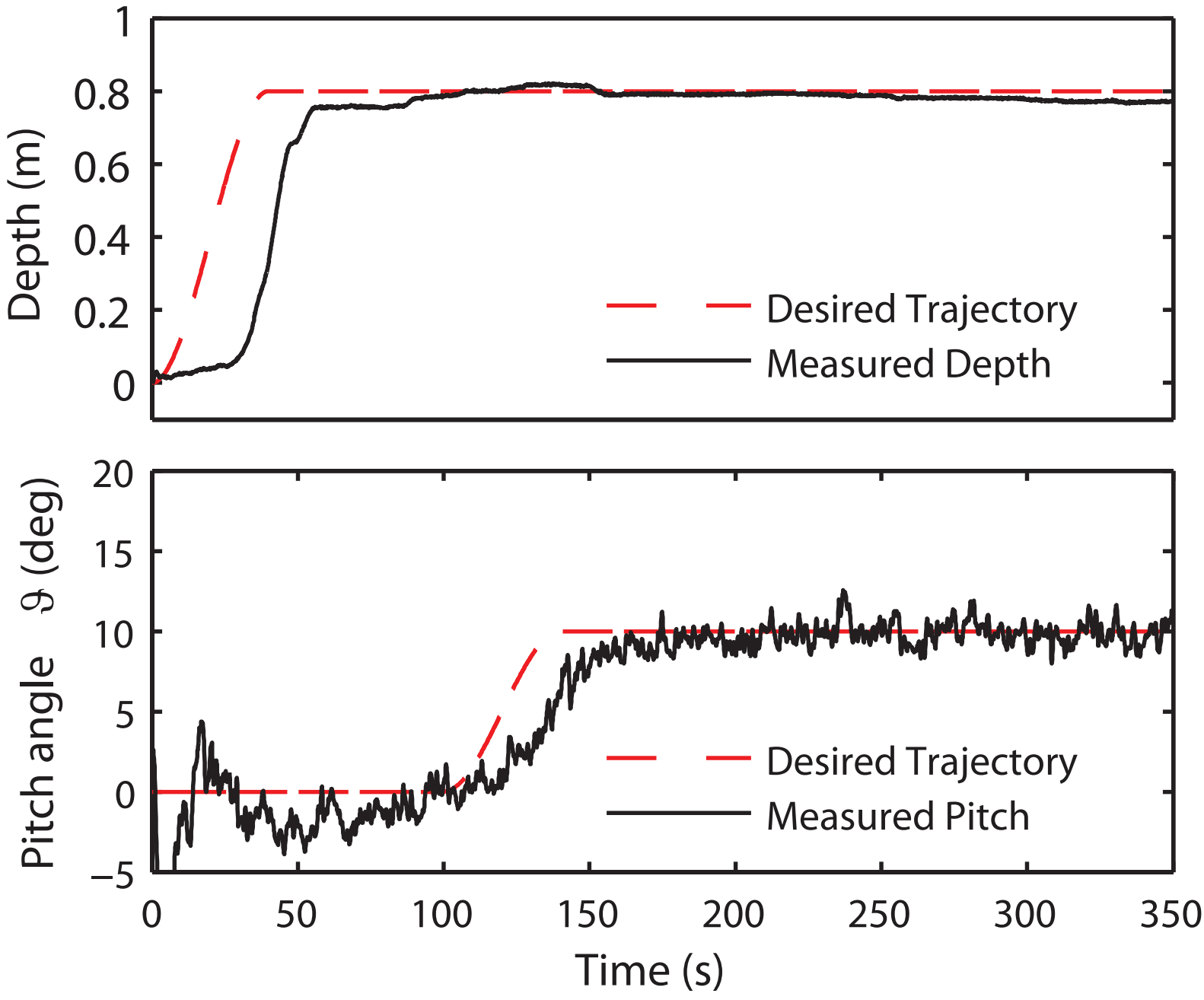
Depth (m)
1
0.8
0.6
0.4
0.2
0
Desired Trajectory
Measured Depth
Pitch angle ϑ (deg)
20
15
10
5
0
−5
Desired Trajectory
Measured Pitch
0
50
100
150
200
250
300
350
Time (s)

Figure

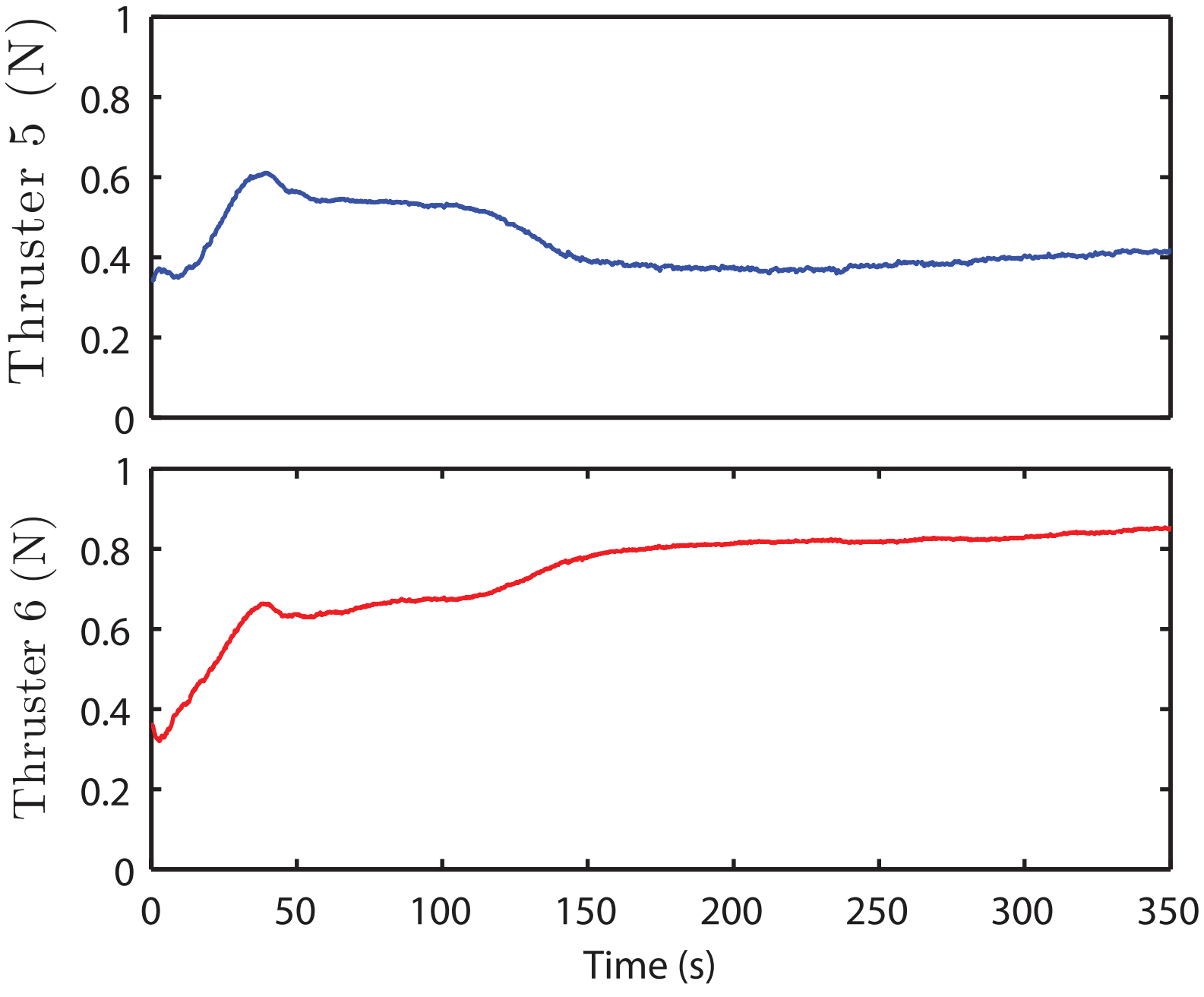
Thruster 5 (N)
Thruster 6 (N)
0
0.2
0.4
0.6
0.8
1
0
50
100
150
200
250
300
350
Time (s)

Figure

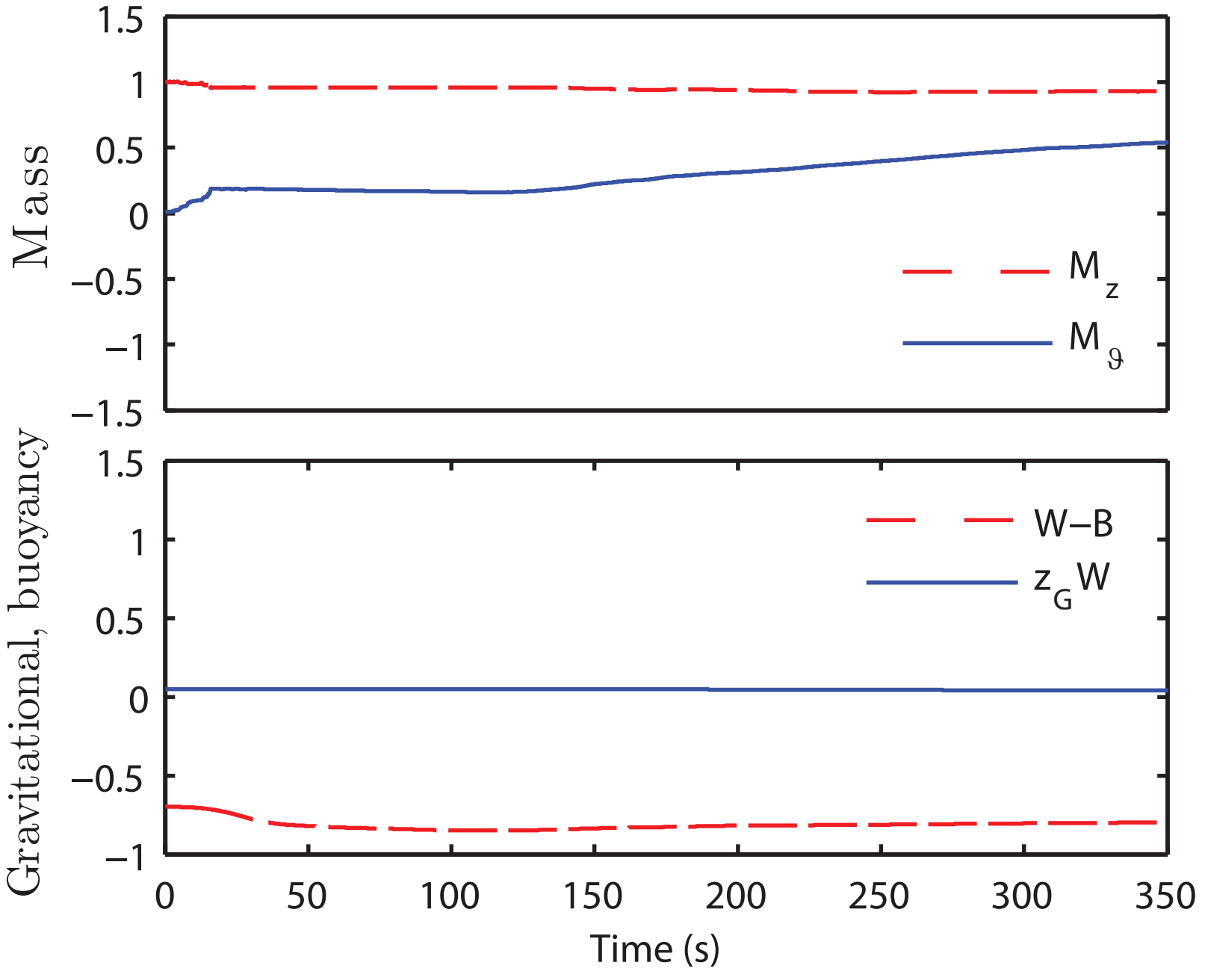
Mass
1.5
1
0.5
0
−0.5
−1
−1.5
M z
M ϑ
Gravitational, buoyancy
1.5
1
0.5
0
−0.5
−1
W−B
z G W
0
50
100
150
200
250
300
350
Time (s)

Figure

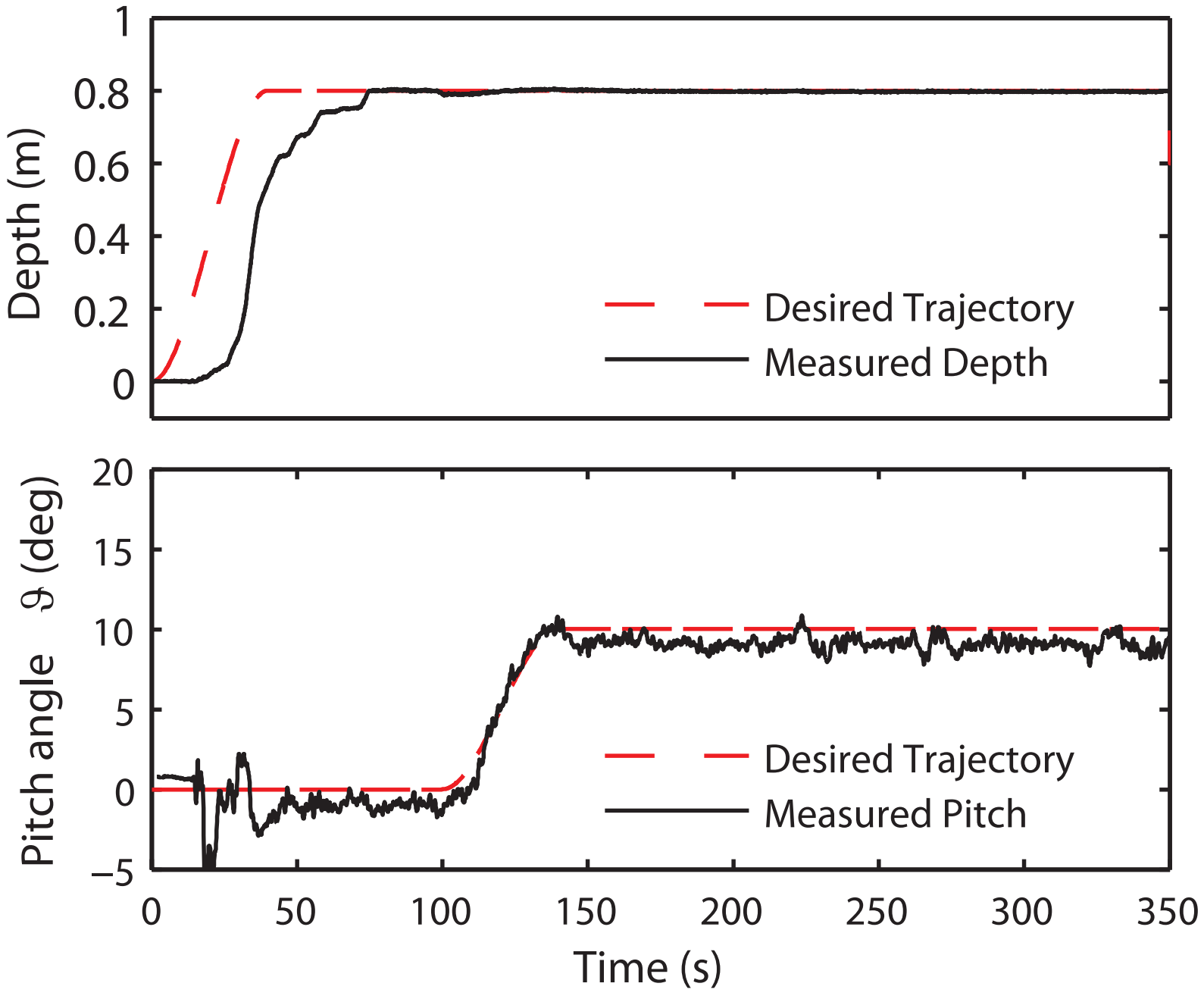
Depth (m)
1
0.8
0.6
0.4
0.2
0
Desired Trajectory
Measured Depth
Pitch angle ϑ (deg)
20
15
10
5
0
−5
Desired Trajectory
Measured Pitch
0
50
100
150
200
250
300
350
Time (s)

Figure

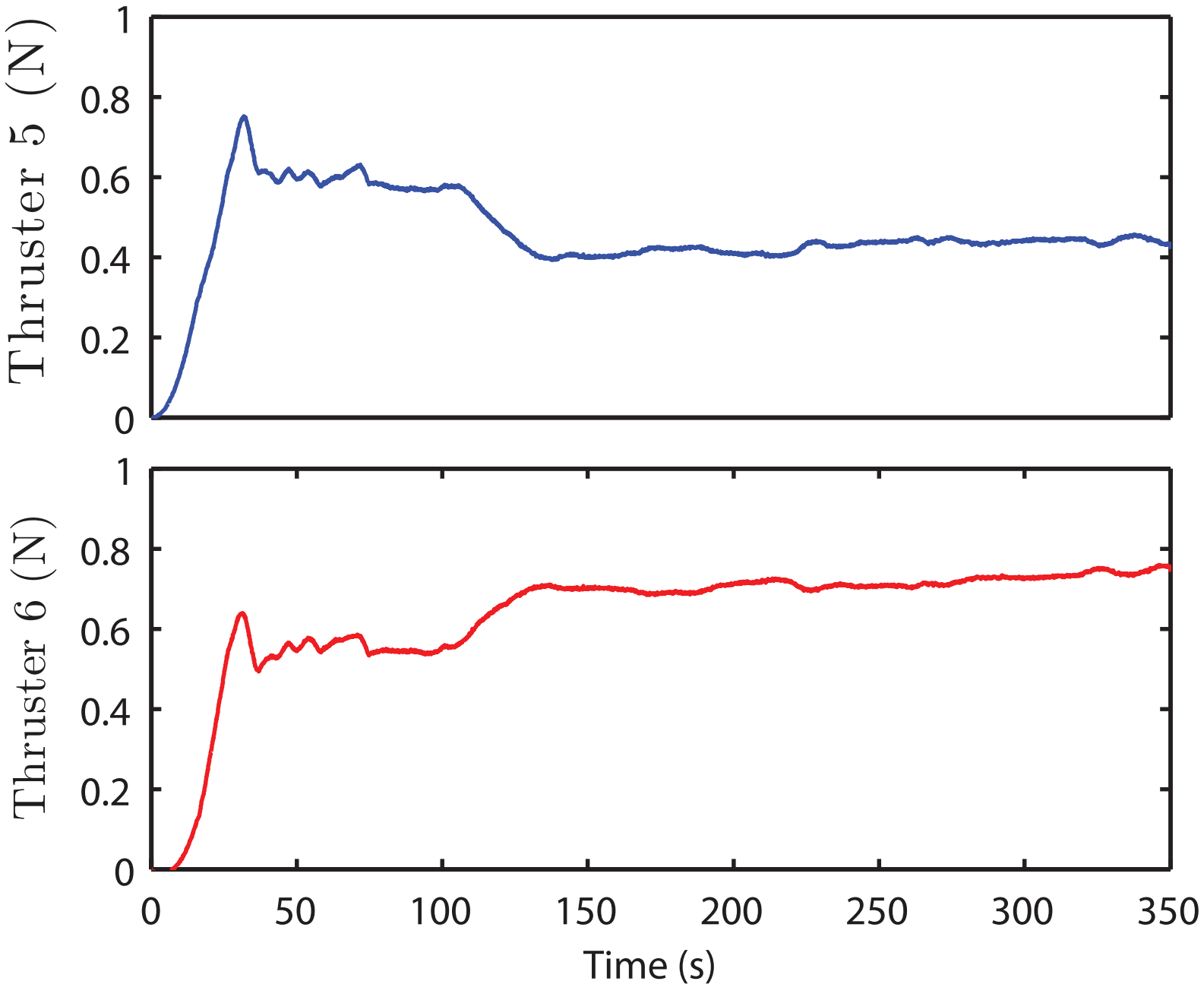
Thruster 5 (N)
1
0.8
0.6
0.4
0.2
0
Thruster 6 (N)
1
0.8
0.6
0.4
0.2
0
0
50
100
150
200
250
300
350
Time (s)

Figure

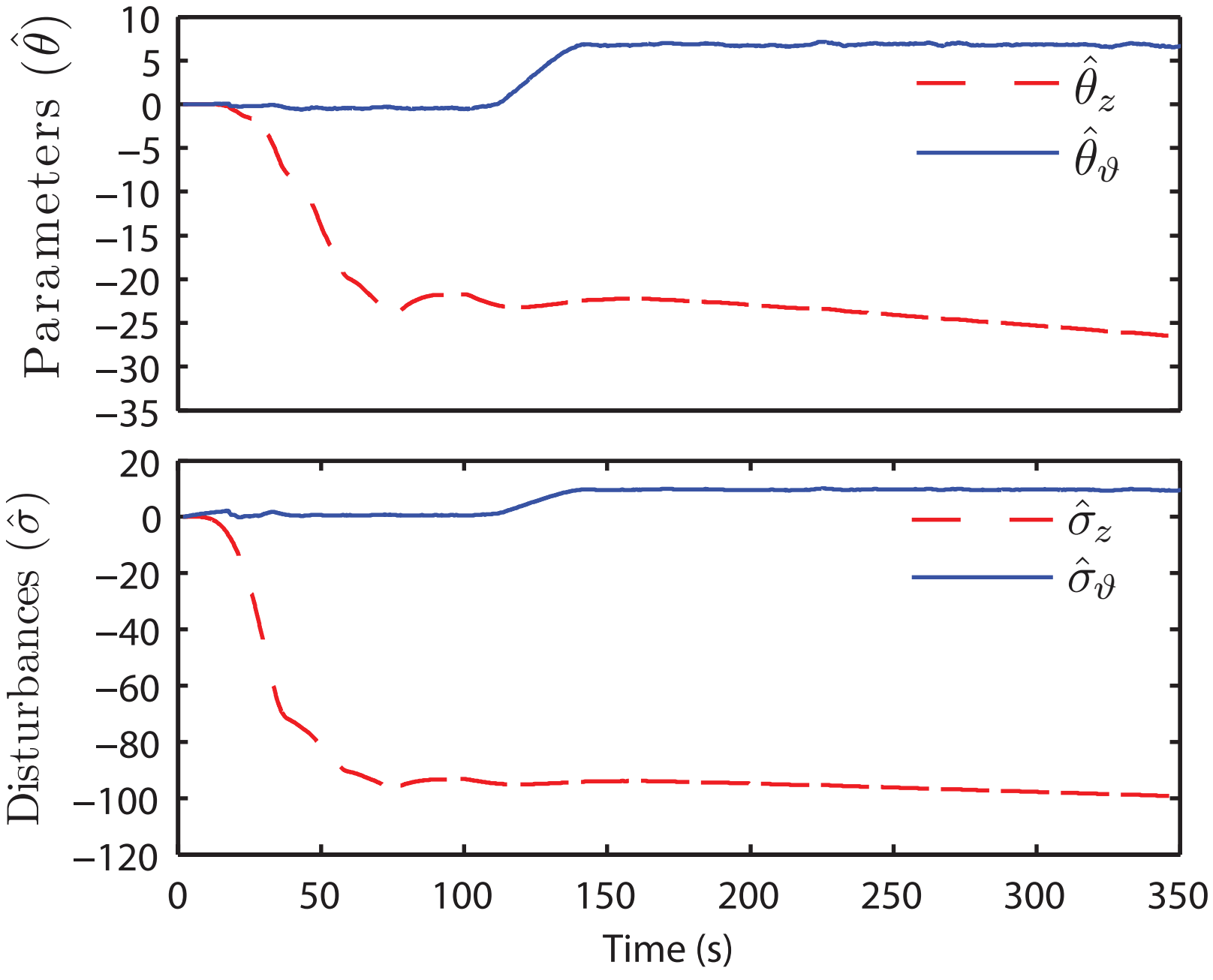
Parameters $(\hat{\theta})$
10
5
0
−5
−10
−15
−20
−25
−30
−35
$\hat{\theta}_z$
$\hat{\theta}_\vartheta$
Disturbances $(\hat{\sigma})$
20
0
−20
−40
−60
−80
−100
−120
$\hat{\sigma}_z$
$\hat{\sigma}_\vartheta$
0
50
100
150
200
250
300
350
Time (s)

Figure

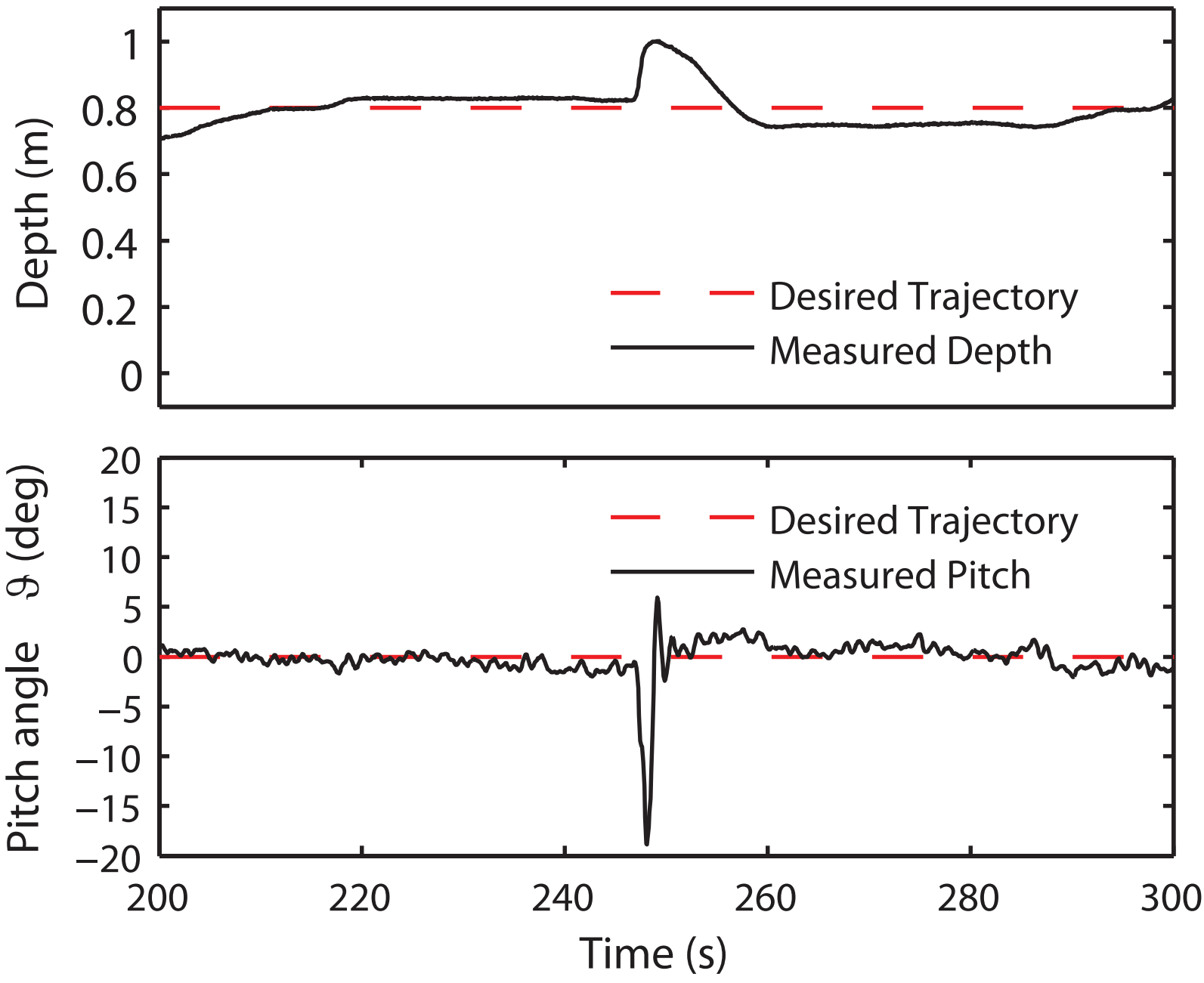
Depth (m)
1
0.8
0.6
0.4
0.2
0
Desired Trajectory
Measured Depth
Pitch angle ϑ (deg)
20
15
10
5
0
−5
−10
−15
−20
Desired Trajectory
Measured Pitch
200
220
240
260
280
300
Time (s)

Figure

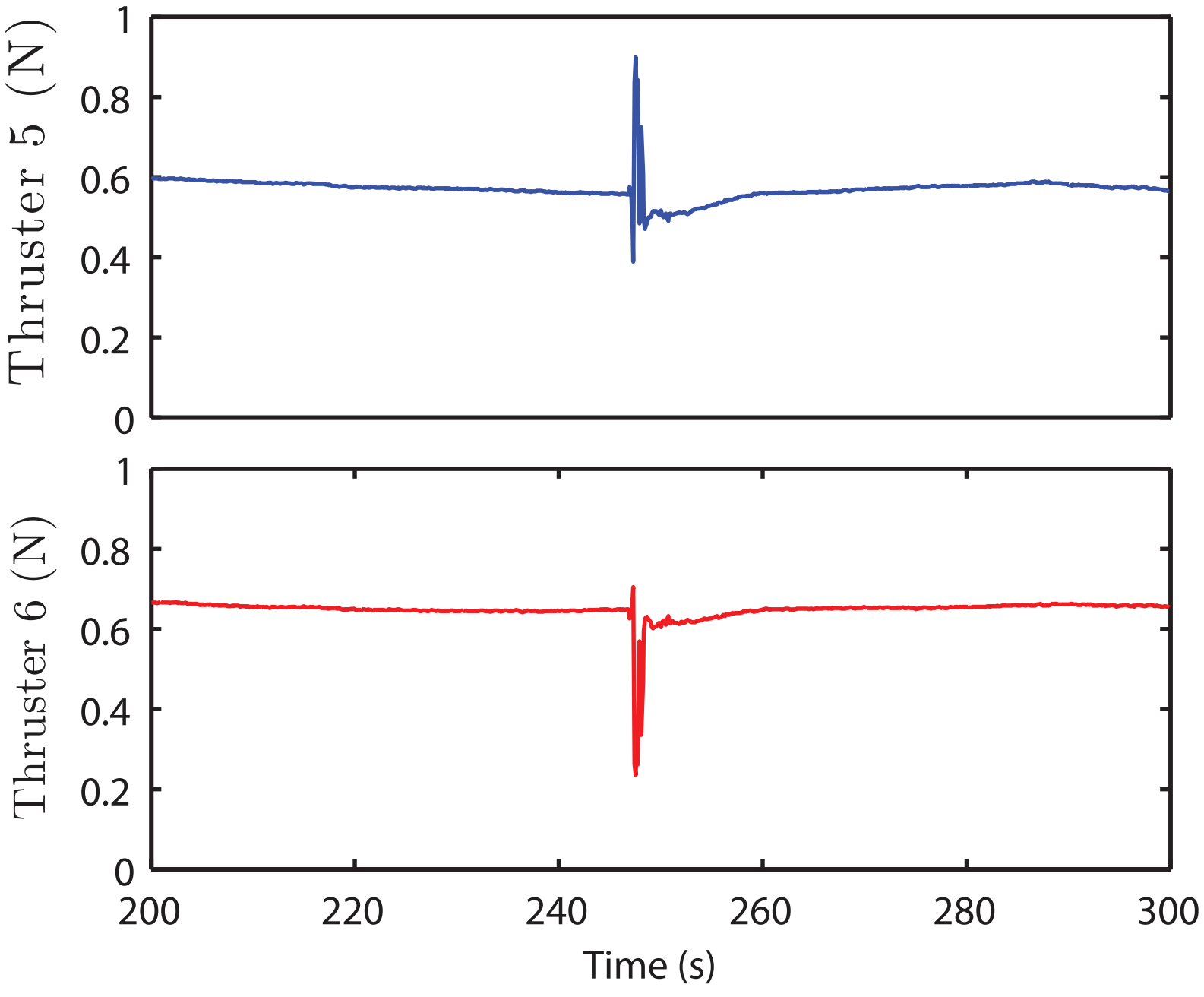
Thruster 5 (N)
1
0.8
0.6
0.4
0.2
0
Thruster 6 (N)
1
0.8
0.6
0.4
0.2
0
200
220
240
260
280
300
Time (s)

Figure

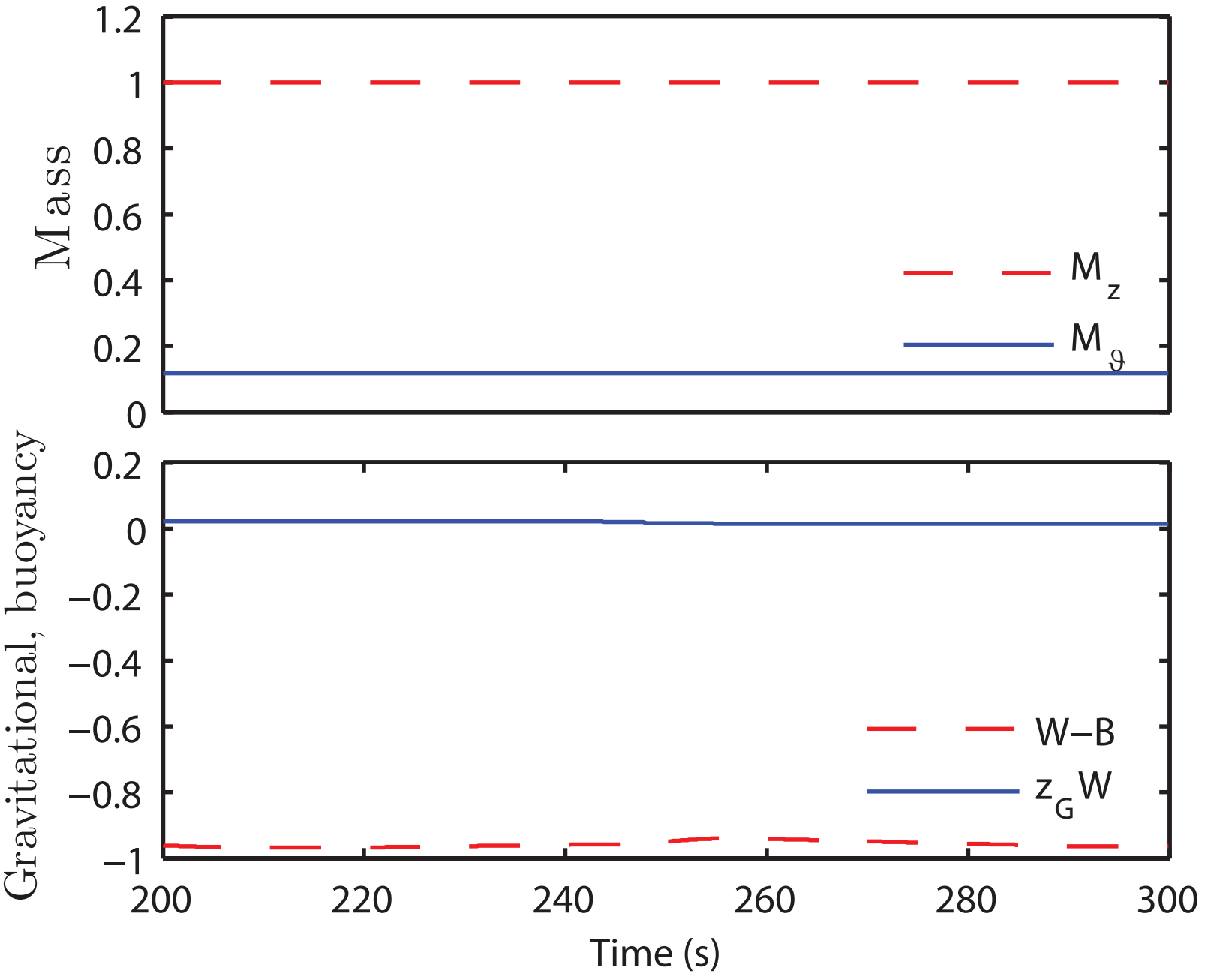
1.2
1
0.8
0.6
0.4
0.2
0
Mass
M z
M ϑ
0.2
0
−0.2
−0.4
−0.6
−0.8
−1
Gravitational, buoyancy
W−B
z G W
200
220
240
260
280
300
Time (s)

Figure

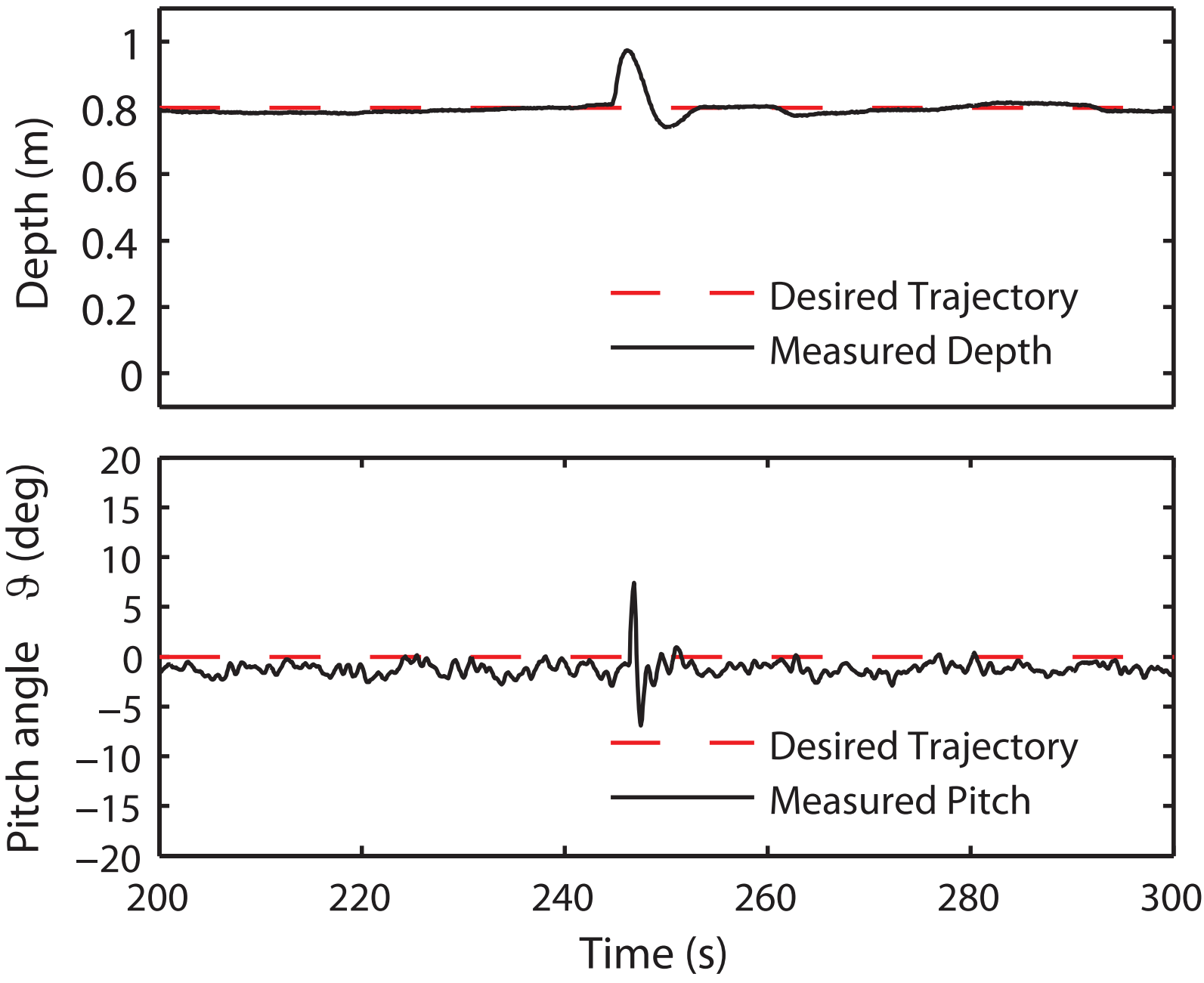
Depth (m)
1
0.8
0.6
0.4
0.2
0
Desired Trajectory
Measured Depth
Pitch angle ϑ (deg)
20
15
10
5
0
−5
−10
−15
−20
Desired Trajectory
Measured Pitch
200
220
240
260
280
300
Time (s)

Figure

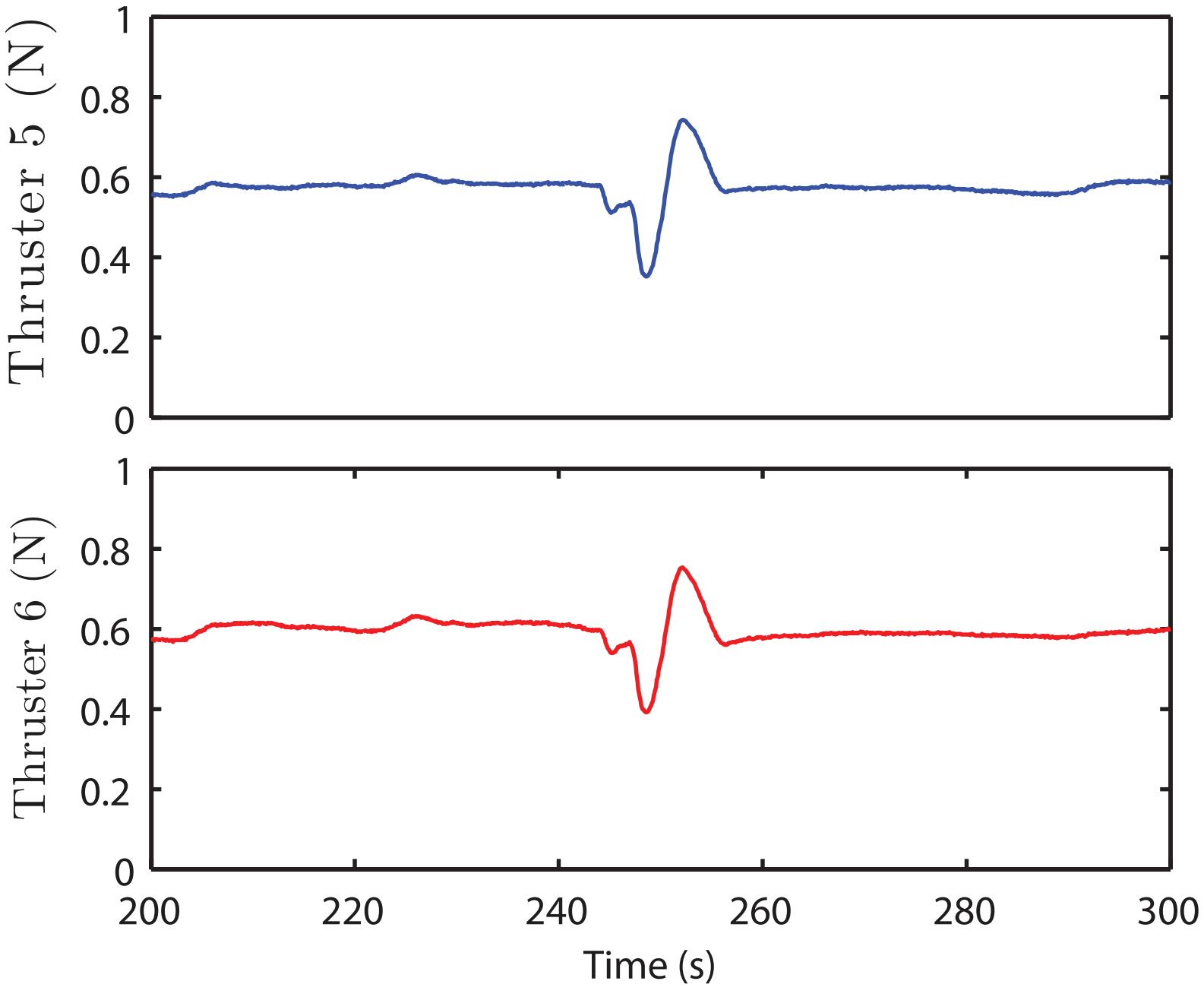
Thruster 5 (N)
1
0.8
0.6
0.4
0.2
0
Thruster 6 (N)
1
0.8
0.6
0.4
0.2
0
200
220
240
260
280
300
Time (s)

Figure

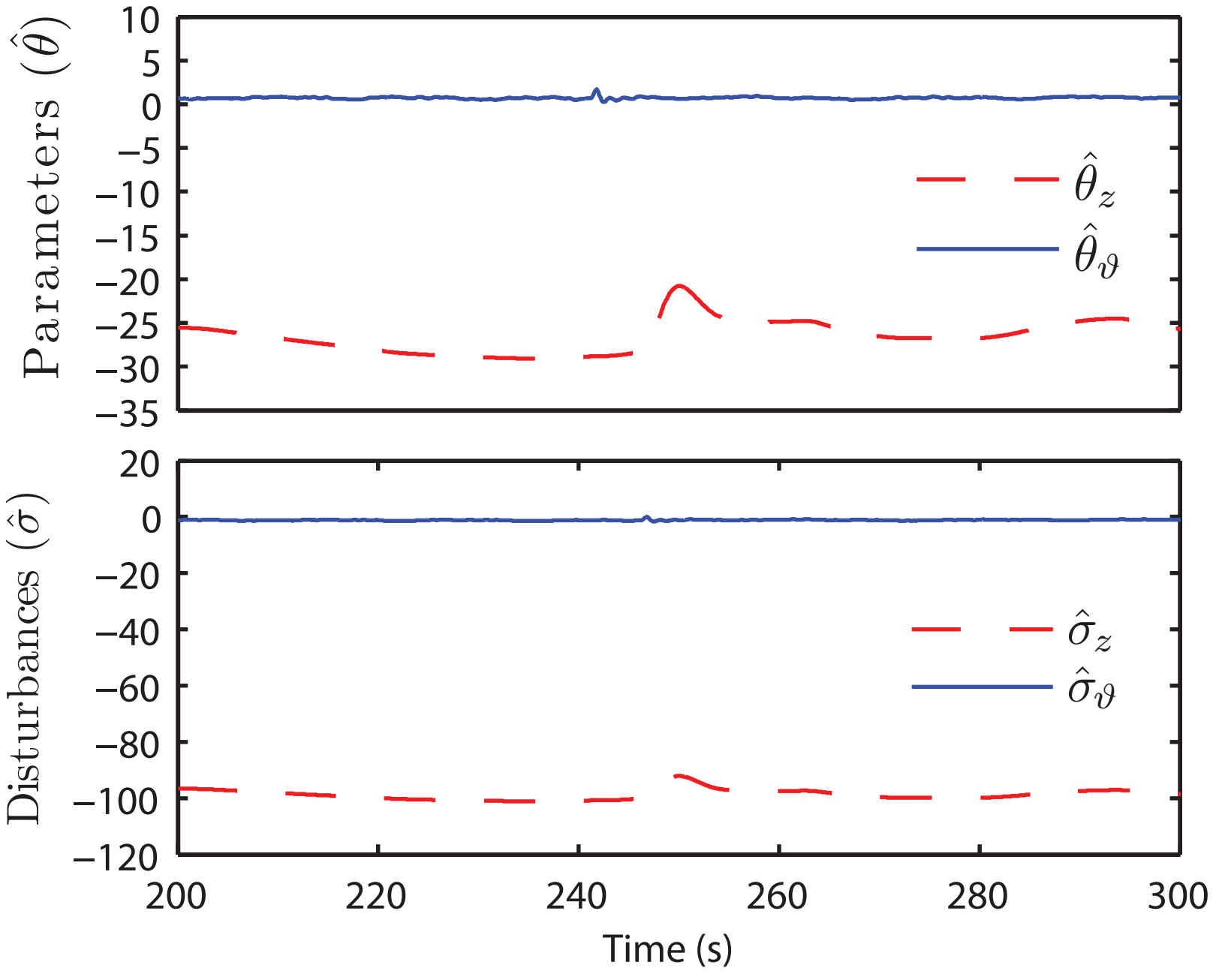
Parameters ($\hat{\theta}$)
10
5
0
−5
−10
−15
−20
−25
−30
−35
$\hat{\theta}_z$
$\hat{\theta}_\vartheta$
Disturbances ($\hat{\sigma}$)
20
0
−20
−40
−60
−80
−100
−120
$\hat{\sigma}_z$
$\hat{\sigma}_\vartheta$
200
220
240
260
280
300
Time (s)

Figure

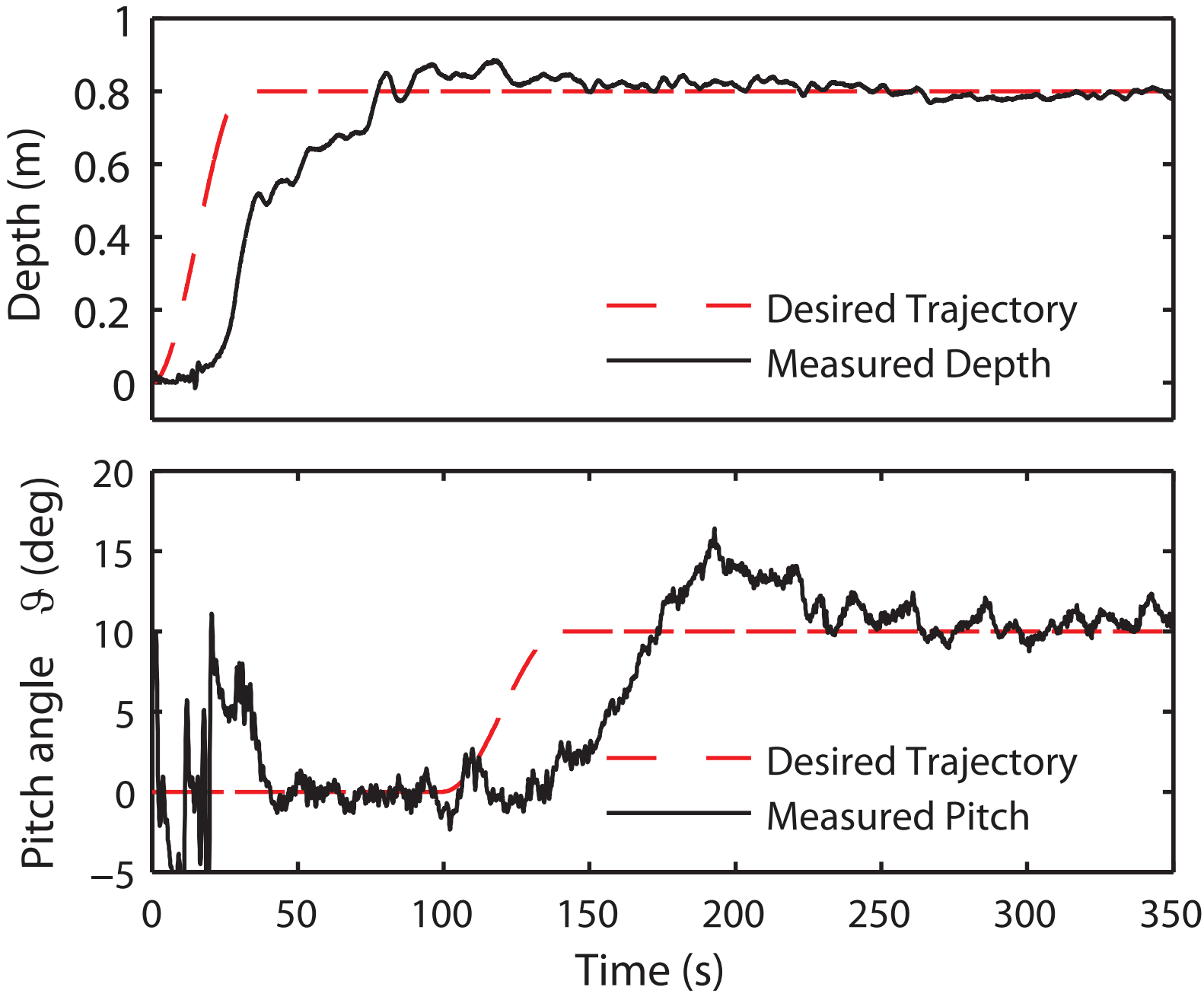
Depth (m)
1
0.8
0.6
0.4
0.2
0
Desired Trajectory
Measured Depth
Pitch angle ϑ (deg)
20
15
10
5
0
−5
Desired Trajectory
Measured Pitch
0
50
100
150
200
250
300
350
Time (s)

Figure

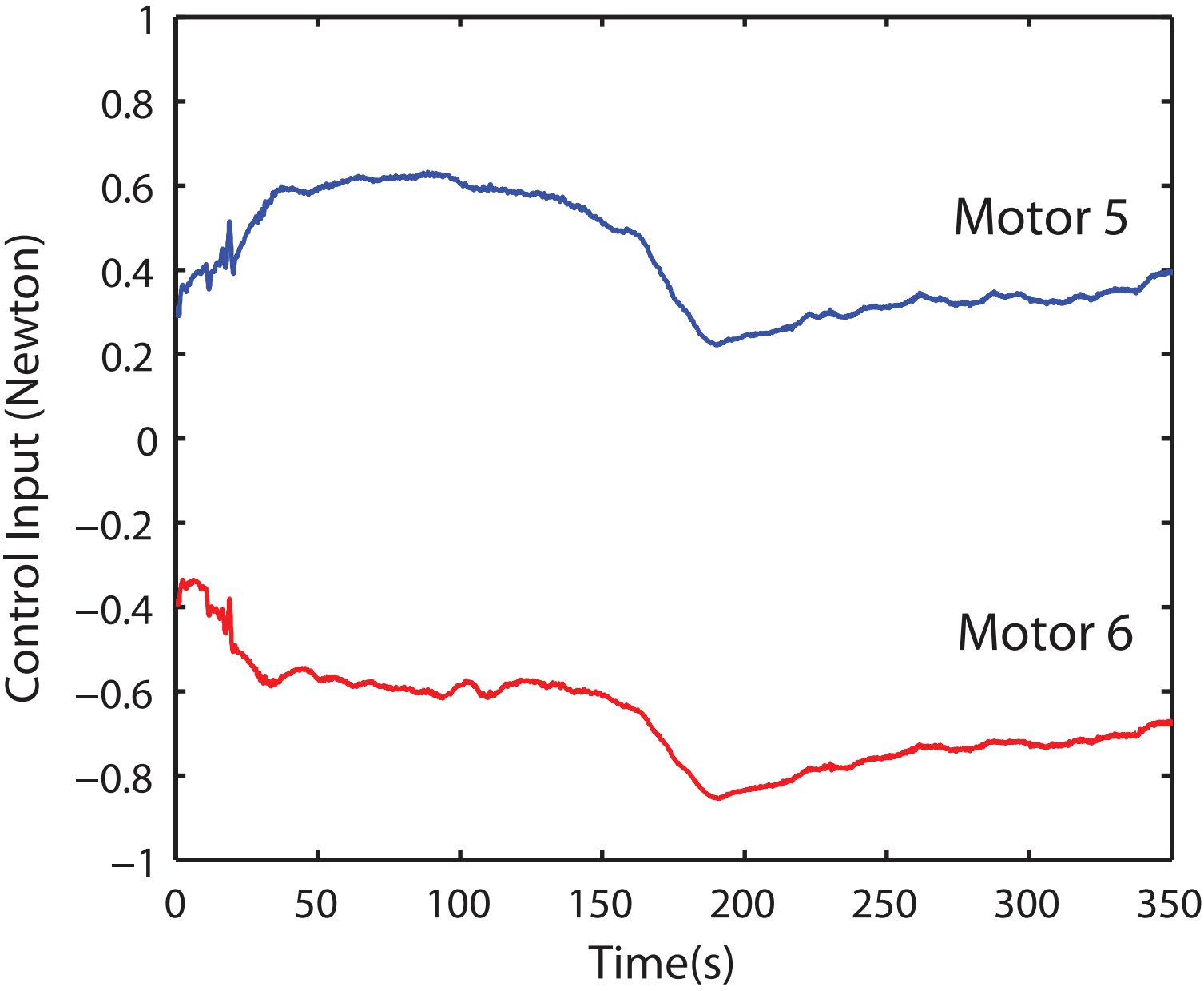
Control Input (Newton)
1
0.8
0.6
0.4
0.2
0
−0.2
−0.4
−0.6
−0.8
−1
0
50
100
150
200
250
300
350
Time(s)
Motor 5
Motor 6

Figure

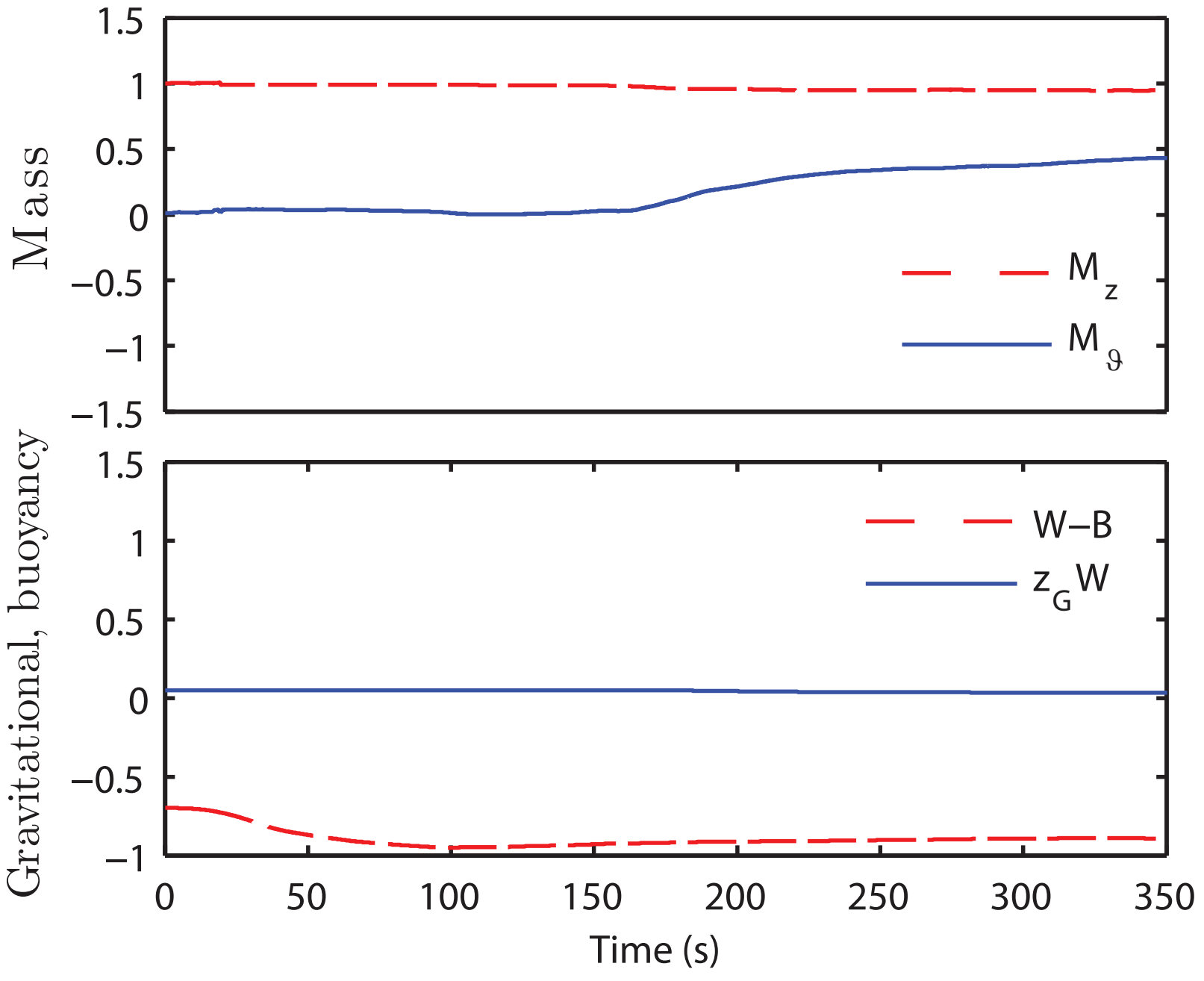
Mass
1.5
1
0.5
0
−0.5
−1
−1.5
M z
M ϑ
Gravitational, buoyancy
1.5
1
0.5
0
−0.5
−1
W−B
z G W
0
50
100
150
200
250
300
350
Time (s)

Figure

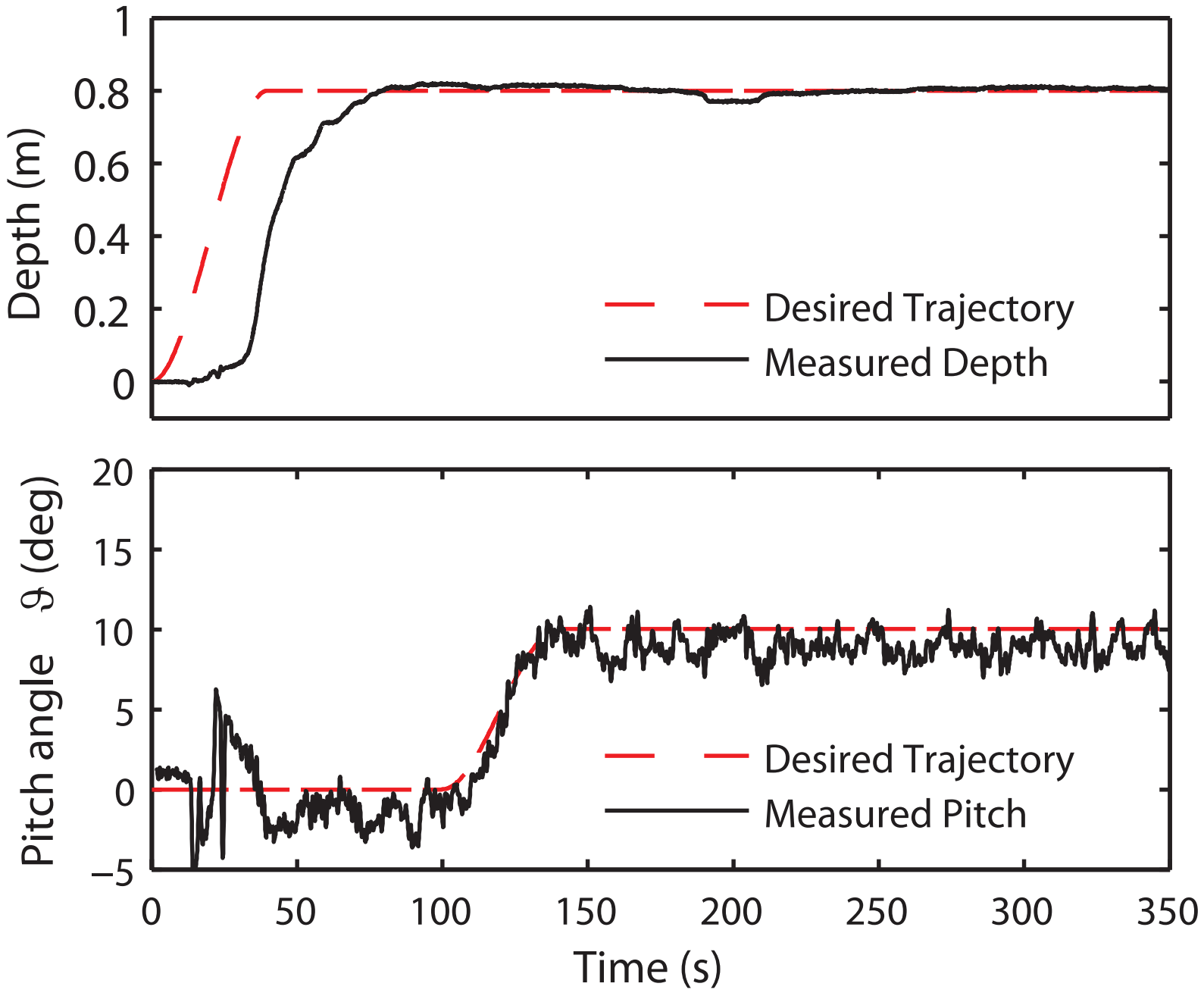
Depth (m)
1
0.8
0.6
0.4
0.2
0
Desired Trajectory
Measured Depth
Pitch angle ϑ (deg)
20
15
10
5
0
−5
Desired Trajectory
Measured Pitch
0
50
100
150
200
250
300
350
Time (s)

Figure

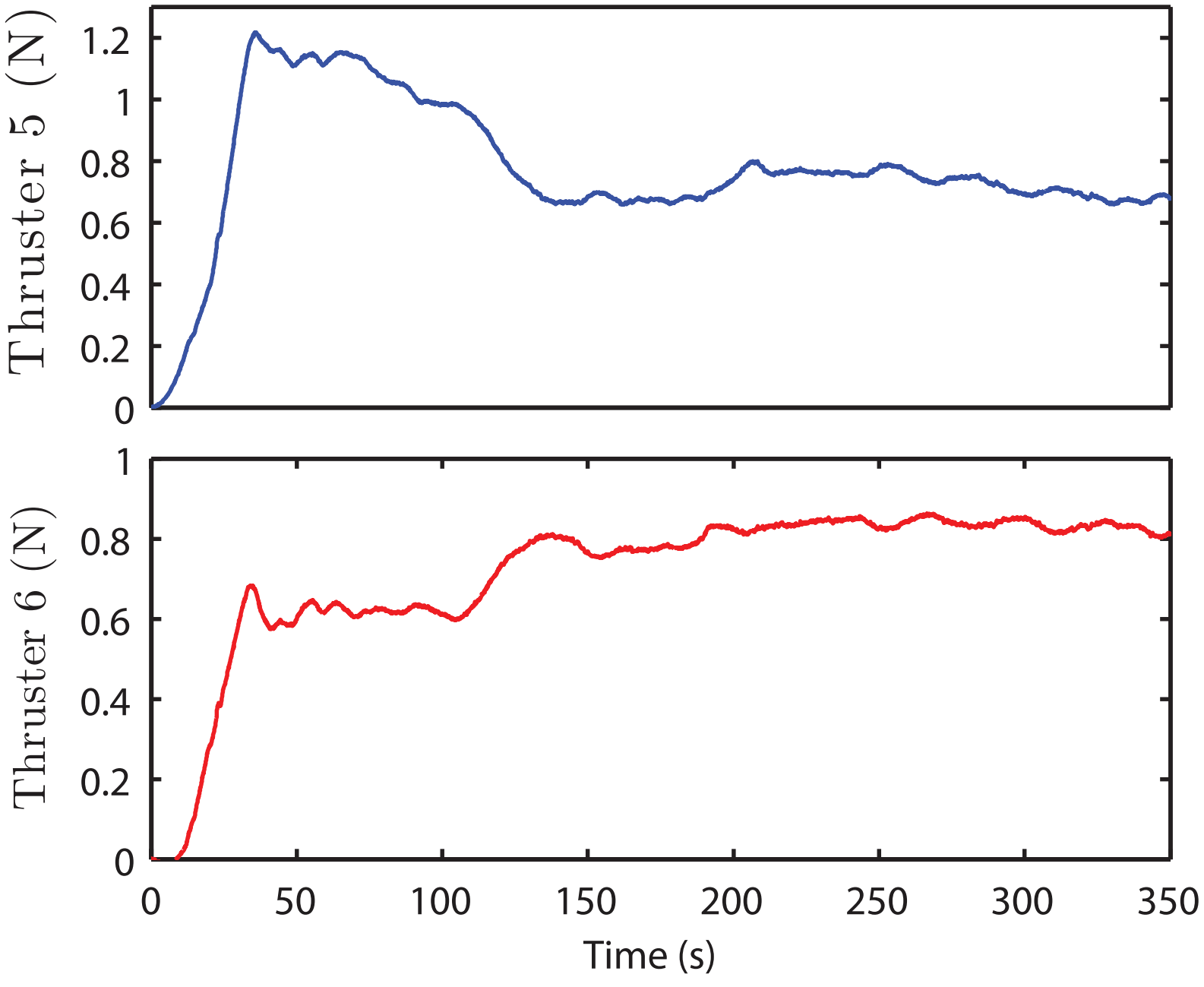
Thruster 5 (N)
1.2
1
0.8
0.6
0.4
0.2
0
Thruster 6 (N)
1
0.8
0.6
0.4
0.2
0
0
50
100
150
200
250
300
350
Time (s)

Figure

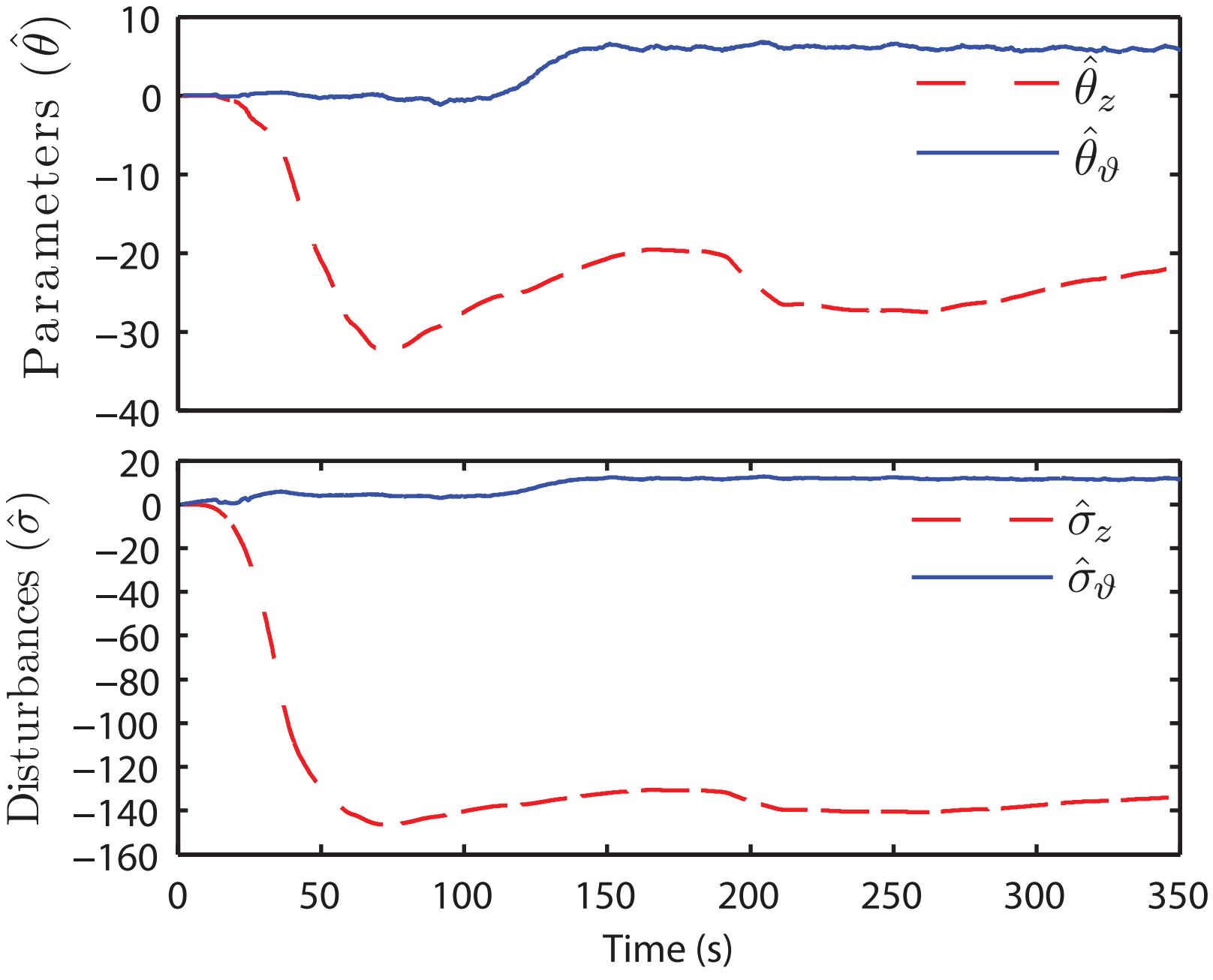
Parameters $(\hat{\theta})$
10
0
−10
−20
−30
−40
$\hat{\theta}_z$
$\hat{\theta}_\vartheta$
Disturbances $(\hat{\sigma})$
20
0
−20
−40
−60
−80
−100
−120
−140
−160
$\hat{\sigma}_z$
$\hat{\sigma}_\vartheta$
0
50
100
150
200
250
300
350
Time (s)